Plasma membrane domain organization regulates EGFR signaling in tumor cells

Patrick Lajoie,[1] Emily A. Partridge,[2] Ginette Guay,[3] Jacky G. Goetz,[1,3] Judy Pawling,[2] Annick Lagana,[4] Bharat Joshi,[1] James W. Dennis,[2,5,6] and Ivan R. Nabi[1]

[1]Department of Cellular and Physiological Sciences, Life Sciences Institute, University of British Columbia, Vancouver, British Columbia V6T 1Z3, Canada
[2]Samuel Lunenfeld Research Institute, Mount Sinai Hospital, Toronto, Ontario M5G 1X5, Canada
[3]Department of Pathology and Cell Biology, Université de Montréal, Montreal, Quebec H3C 3J7, Canada
[4]Biotechnology Research Institute, National Research Council of Canada, Montreal, Quebec H4P 2R2, Canada
[5]Department of Medical Genetics and [6]Department of Laboratory Medicine and Pathology, University of Toronto, Toronto, Ontario M5G 1L5, Canada

Macromolecular complexes exhibit reduced diffusion in biological membranes; however, the physiological consequences of this characteristic of plasma membrane domain organization remain elusive. We report that competition between the galectin lattice and oligomerized caveolin-1 microdomains for epidermal growth factor (EGF) receptor (EGFR) recruitment regulates EGFR signaling in tumor cells. In mammary tumor cells deficient for Golgi β1,6*N*-acetylglucosaminyltransferase V (Mgat5), a reduction in EGFR binding to the galectin lattice allows an increased association with stable caveolin-1 cell surface microdomains that suppresses EGFR signaling. Depletion of caveolin-1 enhances EGFR diffusion, responsiveness to EGF, and relieves Mgat5 deficiency–imposed restrictions on tumor cell growth. In Mgat5$^{+/+}$ tumor cells, EGFR association with the galectin lattice reduces first-order EGFR diffusion rates and promotes receptor interaction with the actin cytoskeleton. Importantly, EGFR association with the lattice opposes sequestration by caveolin-1, overriding its negative regulation of EGFR diffusion and signaling. Therefore, caveolin-1 is a conditional tumor suppressor whose loss is advantageous when β1,6GlcNAc-branched N-glycans are below a threshold for optimal galectin lattice formation.

Introduction

The plasma membrane of the cell is organized into cell surface domains that include clathrin-coated pits, lipid rafts, and caveolae. Lipid rafts have been proposed to be transient and dynamic nanodomains of <10 nm in size (Mayor and Rao, 2004; for review see Hancock, 2006). Caveolae are invaginated lipid raft macrodomains (50–150 nm) whose stability at the plasma membrane is attributable, in large part, to the formation of highly stable oligomers of their coat protein, caveolin-1 (Thomsen et al., 2002; van Deurs et al., 2003; Parton et al., 2006). Clathrin-coated pits (100–150 nm) internalize rapidly upon formation at the same plasma membrane site, and their lateral cell surface mobility is enhanced by actin cytoskeleton depolymerization (Gaidarov et al., 1999). The membrane skeleton, which is associated with the cytoplasmic face of the plasma membrane, is composed of a meshwork of actin filaments and associated proteins that form fences and pickets that restrict molecular diffusion and partition the membrane into compartments that vary in size from 50 to several hundred nanometers in size. Large-scale movements require the traversing of these compartmental boundaries via a process called hop diffusion, providing an explanation for the reduced diffusion of macromolecular complexes in biological membranes (Heuser and Kirschner, 1980; Edidin et al., 1991; Jacobson et al., 1995; Kusumi et al., 2005b; Morone et al., 2006). However, the identification of physiological processes regulated by plasma membrane domain compartmentalization remains limited.

Molecular cross-linking of raft components has been proposed to generate stabilized domains that promote transmembrane signaling and interaction with the cytoskeleton (Simons and Toomre, 2000; Kusumi et al., 2004). Clustering of the glycosyl-phosphatidylinositol–anchored receptor CD59 was recently shown to result in the transient recruitment of Gαi2 and Lyn and immobilization through binding to F-actin, which was termed stimulation-induced temporary arrest of lateral diffusion (STALL); the recruitment of PLCγ to CD59 clusters undergoing STALL results in local IP3-Ca^{2+} signaling events

Correspondence to Ivan R. Nabi: ivan.robert.nabi@ubc.ca

Abbreviations used in this paper: CT-B, cholera toxin b subunit; EGFR, EGF receptor; EMT, epithelial-mesenchymal transition; LatA, latrunculin A; MMTV, mouse mammary tumor virus; mRFP, monomeric RFP; PyMT, polyoma middle T antigen.

The online version of this article contains supplemental material.

The Journal of Cell Biology, Vol. 179, No. 2, October 22, 2007 341–356
http://www.jcb.org/cgi/doi/10.1083/jcb.200611106

(Suzuki et al., 2007a,b). Single-particle tracking analysis has shown that movement of cell surface–bound murine polyoma-like virus particles is actin restricted, cholesterol dependent, and not associated with caveolae or clathrin-coated pits (Ewers et al., 2005). However, the transient anchorage of cross-linked glycosylphosphatidylinositol–anchored proteins was found to be dependent on caveolin in addition to cholesterol and Src family kinases (Chen et al., 2006). Ras clustering upon activation supports a role for macromolecular complex formation in signal transduction (Murakoshi et al., 2004; Plowman et al., 2005).

Glycan-based domains generated by galectin binding to cell surface glycoproteins have been proposed (Brewer et al., 2002). The *Mgat5* gene encodes β1,6*N*-acetylglucosaminyltransferase V (GlcNAc-TV), a Golgi-processing enzyme that modifies N-glycans, generating high affinity ligands for galectins (Demetriou et al., 2001). The galectins are a family of β-galactoside–binding proteins with affinities for N-glycans proportional to GlcNAc branching (Hirabayashi et al., 2002) that can cross-link glycoproteins to form molecular lattices (Ahmad et al., 2004). Close interactions of galectin-3 on the cell surface have recently been shown by fluorescence resonance energy transfer, demonstrating that galectin-3 can oligomerize to form a lattice (Nieminen et al., 2007). We have shown that binding of Mgat5-modified N-glycans on EGF and TGF-β receptors to galectin-3 opposes receptor loss to constitutive endocytosis and, thereby, sensitizes cells to cytokines. Blocking clathrin-coated pit endocytosis with potassium depletion and lipid raft endocytosis with nystatin rescued cytokine EGF and TGF-β sensitivity in Mgat5$^{-/-}$ tumor cells (Partridge et al., 2004). This suggested that galectin binding protects receptors from negative regulation through interaction with clathrin-coated pits and lipid rafts. Herein, we demonstrate that the reduction of EGF receptor (EGFR) lateral mobility by Mgat5-dependent galectin-mediated cross-linking limits interaction of the receptor with stable inhibitory domains of oligomerized caveolin. Our data indicate that recruitment to positive regulatory Mgat5/galectin-dependent macromolecular complexes limits the large-scale macrodiffusion of EGFR, effectively competing with receptor recruitment to other plasma membrane domains.

Mgat5 gene expression and its β1,6GlcNAc-branched N-glycan products increase with oncogenic transformation in human cancers of the breast and colon and contribute directly to tumor progression and metastasis in mice (Dennis et al., 2002). In transgenic mice expressing the polyoma middle T antigen (PyMT) transgene under the control of the mouse mammary tumor virus (MMTV) long terminal repeat, Mgat5$^{-/-}$ mice show delayed tumor development and considerably fewer lung metastases compared with their Mgat5$^{+/+}$ littermates (Granovsky et al., 2000). In contrast to the Mgat5$^{-/-}$ background, MMTV-PyMT mammary tumorigenesis is accelerated in Cav1$^{-/-}$ mice (Capozza et al., 2003; Williams et al., 2003).

Cav1 has been shown to act as a negative regulator of growth signaling (Razani et al., 2000; Parton and Simons, 2007) that, via its scaffolding domain (Okamoto et al., 1998; Smart et al., 1999), recruits EGF, PDGF, and TGF-β receptors to caveolae and suppresses responsiveness to these cytokines (Razani et al., 2001; Matveev and Smart, 2002; Di Guglielmo et al., 2003). The CAV1 gene maps to a tumor suppressor locus (D7S522; 7q31.1) that is frequently deleted in human carcinomas, including breast cancer (Williams and Lisanti, 2005). Up to 16% of human breast cancers express a CAV1 P132L mutation that correlates with breast tumor progression and acts as a dominant negative for scaffold domain–dependent growth suppression (Hayashi et al., 2001; Lee et al., 2002). However, contrasting with its apparent tumor suppressor function, Cav1 expression is associated with a poor prognosis in multiple tumor types, including breast tumors (Yang et al., 1999; Suzuoki et al., 2002; Savage et al., 2007).

The demonstration here that Mgat5 expression overrides the tumor suppressor function of Cav1 identifies the latter as a conditional tumor suppressor. The Mgat5-dependent galectin-glycoprotein lattice is a positive signaling environment that regulates EGFR mobility and acts dominantly to protect receptors from negative regulation and immobilization through interaction with oligomerized Cav1. Mgat5-dependent expression of the galectin lattice relieves Cav1 suppression in Mgat5$^{+/+}$ PyMT mammary tumor cells, and responsiveness to EGF is rescued in Mgat5$^{-/-}$ tumor cells by reducing Cav1 levels below a threshold. Our results demonstrate the competitive recruitment of EGFR to the extracellular galectin lattice and stable caveolin-1 microdomains and show that the integrity of these domains determines signaling potential and tumor progression.

Results

Reduced Cav1 expression is associated with increased EGFR signaling and tumor growth in Mgat5$^{-/-}$ tumor cells

The majority of PyMT Mgat5$^{-/-}$ tumors are small (<2 cm^3), but a minority (5–10%) of breast tumors in PyMT Mgat5$^{-/-}$ mice display an acceleration of growth, suggesting escape from the suppressive effects of Mgat5 deficiency (Granovsky et al., 2000). Mgat5$^{-/-}$ and escaper Mgat5$^{-/-ESC}$ tumor cell lines were established from small and large tumors, respectively, of MMTV-PyMT Mgat5$^{-/-}$ mice. Compared with Mgat5$^{+/+}$ mammary carcinoma cells, the Mgat5$^{-/-}$ cell line is markedly less sensitive to EGF and TGF-β and is deficient in epithelial-mesenchymal transition (EMT) and fibronectin matrix deposition (Partridge et al., 2004; Lagana et al., 2006). In contrast to Mgat5$^{-/-}$ cells, Mgat5$^{-/-ESC}$ cells display levels of responsiveness to EGF that are comparable with that of wild-type Mgat5$^{+/+}$ cells (Fig. 1 A). However, responsiveness to TGF-β in both Mgat5$^{-/-}$ and Mgat5$^{-/-ESC}$ cells is impaired relative to Mgat5$^{+/+}$ cells (Fig. 1 B). Furthermore, both Mgat5$^{-/-}$ and Mgat5$^{-/-ESC}$ cells are deficient in EMT and fibronectin matrix deposition compared with Mgat5$^{+/+}$ cells (Fig. 1 C). Therefore, the phenotypic rescue of Mgat5$^{-/-ESC}$ cells, which is permissive for tumor growth in the absence of Mgat5, is associated with increased EGFR signaling but not TGF-β signaling, EMT, and fibronectin remodeling associated with Mgat5-dependent invasive tumor cell phenotypes.

Both Mgat5$^{-/-}$ cell lines show the reduced expression of Cav1 relative to Mgat5$^{+/+}$ cells by both quantitative immunofluorescence and Western blotting (Fig. 2, A and B). However,

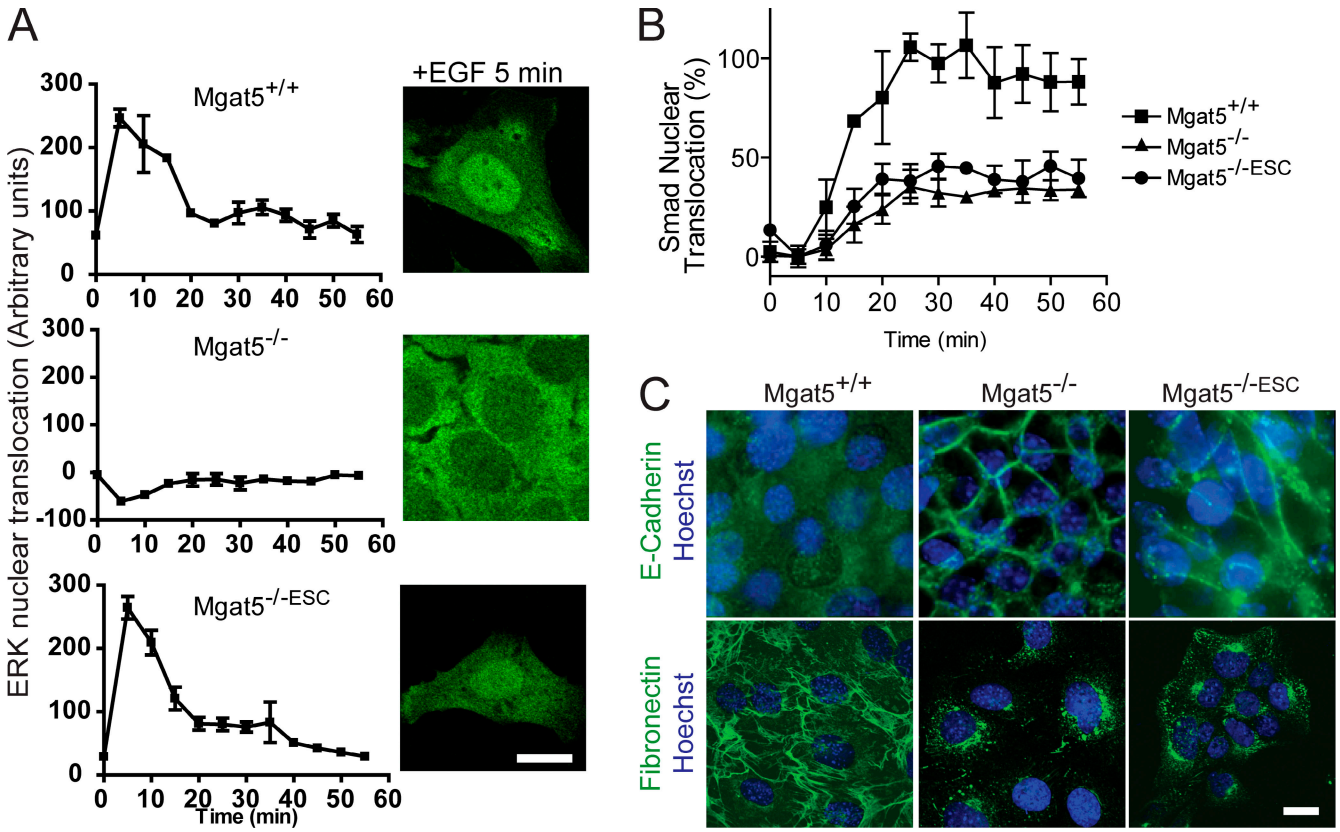

Figure 1. **Mgat5$^{-/-ESC}$ cells show enhanced responsiveness to EGF.** (A) Scan array determination of phospho-Erk nuclear translocation in Mgat5$^{+/+}$, Mgat5$^{-/-}$, and Mgat5$^{-/-ESC}$ cells after stimulation with 100 ng/ml EGF for the indicated times of incubation. Representative phospho-Erk labeling of cells upon EGF stimulation for 5 min are shown. (B) Scan array determination of Smad nuclear translocation in Mgat5$^{+/+}$, Mgat5$^{-/-}$, and Mgat5$^{-/-ESC}$ cells after stimulation with 100 ng/ml TGF-β for the indicated times of incubation. (C) In contrast to Mgat5$^{+/+}$ cells, Mgat5$^{-/-}$ and Mgat5$^{-/-ESC}$ tumor cells display E-cadherin–labeled (green) epithelial cell–cell adherens junctions (top) and little fibronectin organized into fibrils (green). Cell nuclei are labeled with Hoechst (blue). Error bars represent SEM. Bars, 20 μm.

Cav1 and total Cav levels were reduced to a significantly greater extent ($P < 0.05$) in Mgat5$^{-/-ESC}$ than in Mgat5$^{-/-}$ cells (Fig. 2, A and B). Stable infection of Mgat5$^{-/-}$ and Mgat5$^{-/-ESC}$ cells with an Mgat5 expression vector generated rescued Mgat5$^{-/-}$ (Rescue) and Mgat5$^{-/-ESC}$ (ESC-Rescue) cell lines that present restored β1,6GlcNAc-branched N-glycan expression, as verified by labeling with L-PHA–FITC that binds the β1-6 branch of N-glycans (Fig. 2 A). However, Cav1 expression was restored to wild-type levels only upon the rescue of Mgat5$^{-/-}$ but not Mgat5$^{-/-ESC}$ cells (Fig. 2, A and B). In Mgat5$^{+/+}$ cells, Cav1/2 levels were reduced by swainsonine, an α-mannosidase II inhibitor that blocks N-glycan branching, and by β-lactose, a competitive inhibitor of galectin binding at the cell surface (Fig. 2 B). Expression of Mgat5 and the N-glycan processing pathway can therefore impact Cav1. This suggests that Mgat5 and the expression of β1,6GlcNAc-branched N-glycans results in positive feedback to increase Cav1 levels. The failure of Mgat5 to restore Cav1 expression in Mgat5$^{-/-ESC}$ cells suggests that additional genetic modifications may occur in the larger escaper Mgat5$^{-/-}$ tumors that block Cav1 up-regulation and suppression of growth.

Electron microscopic analysis of the cells shows a dramatic reduction in the number of cell surface–associated caveolae in both Mgat5$^{-/-}$ and Mgat5$^{-/-ESC}$ cells relative to Mgat5$^{+/+}$ or Rescue cells that express elevated Cav1 levels without affecting the number of clathrin-coated pits (Fig. 2 C). Cav1 is required for caveolae formation (Fra et al., 1995), suggesting that the threshold level of Cav1 required for caveolae formation is not attained in either Mgat5$^{-/-}$ cell line. To probe for possible functional interactions between Cav1 and the Mgat5-dependent lattice in tumor cells, we compared Cav1 protein levels and mammary tumor volume in MMTV-PyMT Mgat5$^{+/-}$ and MMTV-PyMT Mgat5$^{-/-}$ mice at 12 wk of age. Cav1 levels in Mgat5$^{-/-}$ tumor lysates correlated inversely with increased tumor growth, whereas no correlation with tumor size was observed in Mgat5$^{+/-}$ tumors (Fig. 2 D). Therefore, reduced Cav1 is observed after either chemical disruption of the galectin lattice in Mgat5$^{+/+}$ mammary tumor cells in vitro and spontaneously with tumor progression in PyMT Mgat5$^{-/-}$ tumors in vivo.

Cav1 regulates EGFR mobility and activation in the absence of the galectin lattice

To determine whether lower endogenous Cav1 levels in Mgat5$^{-/-ESC}$ cells were permissive for cytokine responsiveness, Mgat5$^{-/-ESC}$ cells were infected with an adenoviral vector for the expression of Cav1 (Fig. 3 A). Overexpression of Cav1 protein levels in Mgat5$^{-/-ESC}$ cells suppressed EGF-dependent Erk1/2 phosphorylation and nuclear translocation to levels

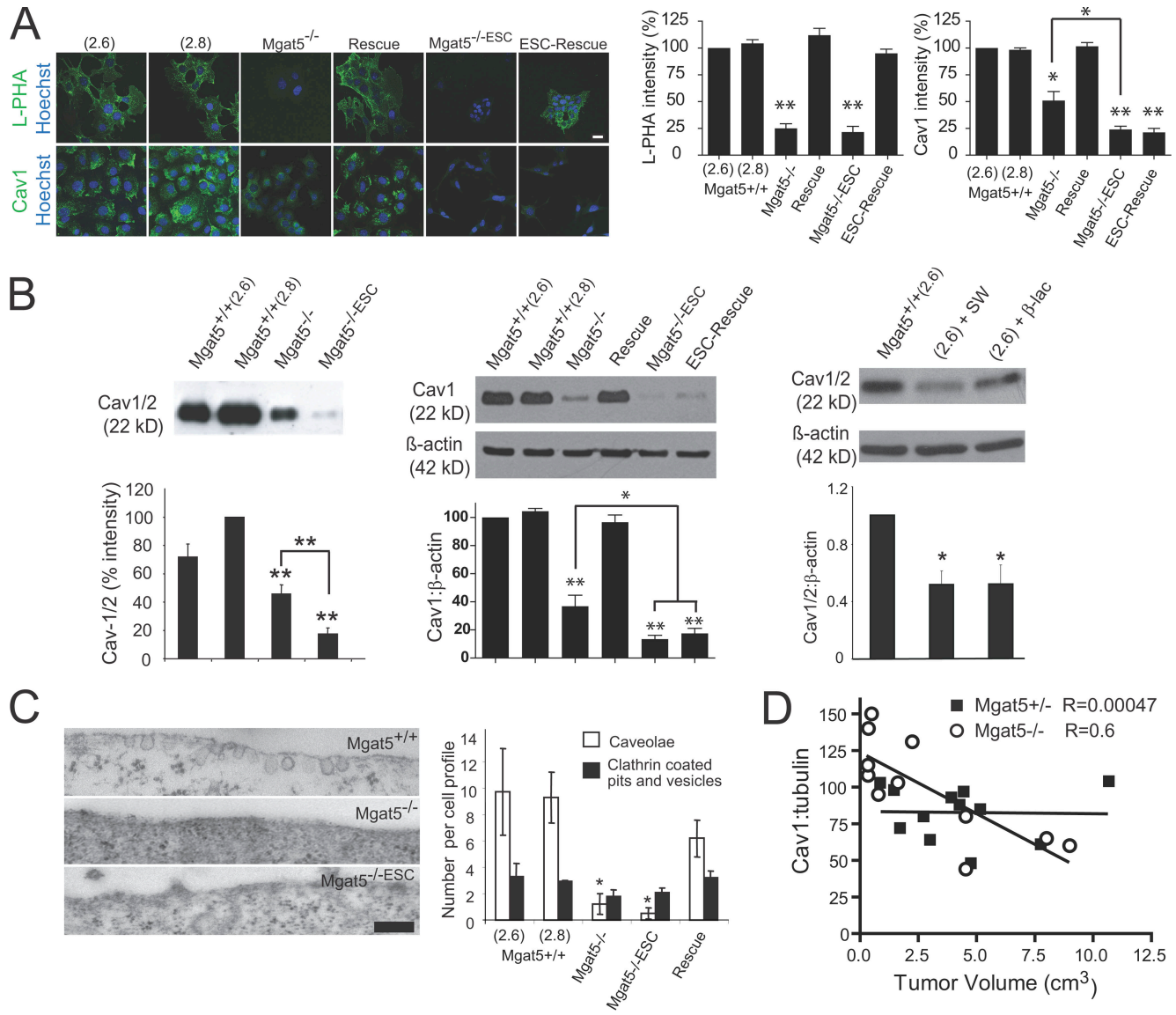

Figure 2. **Reduced Cav1 levels are associated with tumor growth in an Mgat5$^{-/-}$ background.** (A) Mgat5$^{+/+}$, Mgat5$^{-/-}$, Rescue, Mgat5$^{-/-ESC}$, and ESC-Rescue cells were grown on coverslips for 48 h and stained with L-PHA–FITC (green; top) or Cav1 (green; bottom). Cell nuclei are stained with Hoechst (blue). Quantification of L-PHA and Cav1 intensity is shown as a bar graph ($n = 3$; >25 cells per condition). (B) Equal protein amounts of cell lysates from Mgat5$^{+/+}$(2.6) and (2.8), Mgat5$^{-/-}$ and Mgat5$^{-/-ESC}$, and Rescue and ESC-Rescue cells were Western blotted with Cav1/2 or Cav1-specific antibodies as indicated and quantified by densitometry. Mgat5$^{+/+}$ were treated with 1 μM swainsonine (SW) or 20 mM β-lactose (β-lac) for 48 h, blotted for Cav1/2 and β-actin, and quantified by densitometry. (C) Representative electron micrographs of the plasma membrane of Mgat5$^{+/+}$, Mgat5$^{-/-}$, and Mgat5$^{-/-ESC}$ cells. Quantification revealed that both Mgat5-deficient cell lines present reduced the expression of caveolae but not clathrin-coated pits. (D) Spontaneous MMTV-PyMT mammary carcinomas were dissected from 12-wk-old Mgat5$^{+/-}$ and Mgat5$^{-/-}$ mice and subjected to quantitative Western blotting of Cav1 expression levels. Blots were also probed with γ-tubulin as a loading control, and levels of Cav1 were normalized to γ-tubulin levels as determined by densitometry. Results are plotted against tumor volume. *, $P < 0.05$; **, $P < 0.005$ relative to Mgat5$^{+/+}$ unless otherwise indicated. Error bars represent SEM. Bars (A), 20 μm; (C) 0.2 μm.

comparable with untreated Mgat5$^{-/-}$ cells (Fig. 3 A). Cav1 adenoviral infection of Mgat5$^{+/+}$ cells, Rescue, and ESC-Rescue cells did not inhibit EGF responsiveness (Fig. 3 A). This suggests that the expression of β1,6GlcNAc-branched N-glycans protects EGFR from negative regulation by Cav1. This was confirmed by reducing Cav1 with siRNA in Mgat5$^{-/-}$ cells that enhanced the EGF response, but this had no such effect in Mgat5$^{+/+}$, Mgat5$^{-/-ESC}$, or Rescue cell lines (Fig. 3 B). Thus, Mgat5 expression in tumor cells blocks the ability of Cav1 to act as a suppressor of EGFR signaling.

To explore the effects of Cav1 on cell surface raft dynamics, we measured the lateral diffusion rate of GM1-bound cholera toxin b subunit (CT-B) at the cell surface using FRAP at room temperature to limit the internalization of GM1-bound CT-B (Fig. 4 A and Table I; Nichols et al., 2001). Mgat5$^{-/-ESC}$ cells exhibited increased CT-B diffusion relative to the other cell lines. Both the rate of diffusion and fractional recovery of CT-B into the FRAP region was increased in Mgat5$^{-/-ESC}$ cells, suggesting that Cav1 contributes to the reduced mobility of CT-B. Indeed, surface diffusion of CT-B in Mgat5$^{-/-ESC}$ cells was

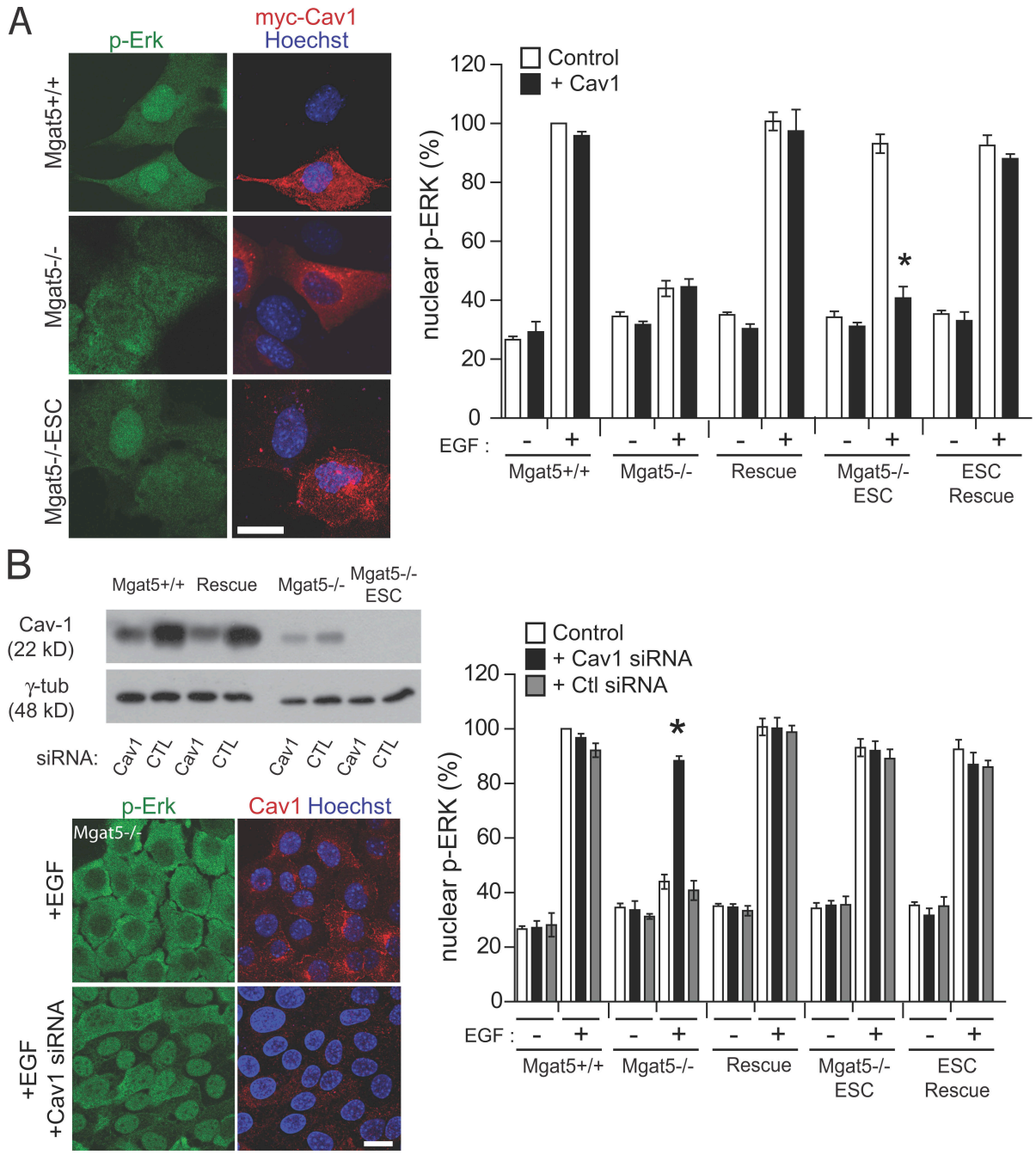

Figure 3. **Cav1 regulation of EGF signaling is selective for an Mgat5$^{-/-}$ background.** (A) Mgat5$^{+/+}$, Mgat5$^{-/-}$, Rescue, Mgat5$^{-/-ESC}$, and ESC-Rescue cells were infected with adenoviruses coding for myc-tagged Cav1 before stimulation with 100 ng/ml EGF for 5 min. Cells were fixed and stained for phospho-Erk (green) and Cav1 (red), and nuclei were identified by Hoechst staining (blue). Quantification of untreated and EGF-treated cells presenting nuclear phospho-Erk is shown as a bar graph (n = 3; >36 cells per condition). (B) Mgat5$^{+/+}$, Rescue, Mgat5$^{-/-}$, and Mgat5$^{-/-ESC}$ cells were treated with Cav1 siRNA, nonspecific (CTL) siRNA, or were left untreated (none) and blotted for Cav1 and γ-tubulin (γ-tub). Mgat5$^{+/+}$, Mgat5$^{-/-}$, Rescue, Mgat5$^{-/-ESC}$, and ESC-Rescue cells were transfected with nonspecific (CTL) siRNA or siRNA coding for Cav1 before stimulation with 100 ng/ml EGF for 5 min. Cells were fixed and stained for phospho-Erk (green) and Cav1 (red), nuclei were identified by Hoechst staining (blue), and representative confocal images of untreated and Cav1 siRNA–treated Mgat5$^{-/-}$ cells are shown. The percentage of cells presenting nuclear phospho-Erk was quantified in untreated and EGF-treated cells that were either untransfected (white bars) or transfected with Cav1 (black bars) or control (gray bars) siRNA and is shown as a bar graph (n = 3; >48 cells per condition). Error bars represent SEM. *, $P < 0.01$ relative to control untransfected cells. Bars, 20 μm.

reduced upon transfection with Cav1–monomeric RFP (mRFP). Conversely, CT-B diffusion was enhanced by Cav1 siRNA treatment of Mgat5$^{+/+}$ and Mgat5$^{-/-}$ cells and presented a profile equivalent to that of Mgat5$^{-/-ESC}$ cells. Therefore, the increased Cav1 expression in Mgat5$^{-/-}$ cells relative to Mgat5$^{-/-ESC}$ cells correlates inversely with raft dynamics.

As observed for CT-B, EGFR-YFP showed enhanced cell surface diffusion and reduced immobile fraction in Mgat5$^{-/-ESC}$

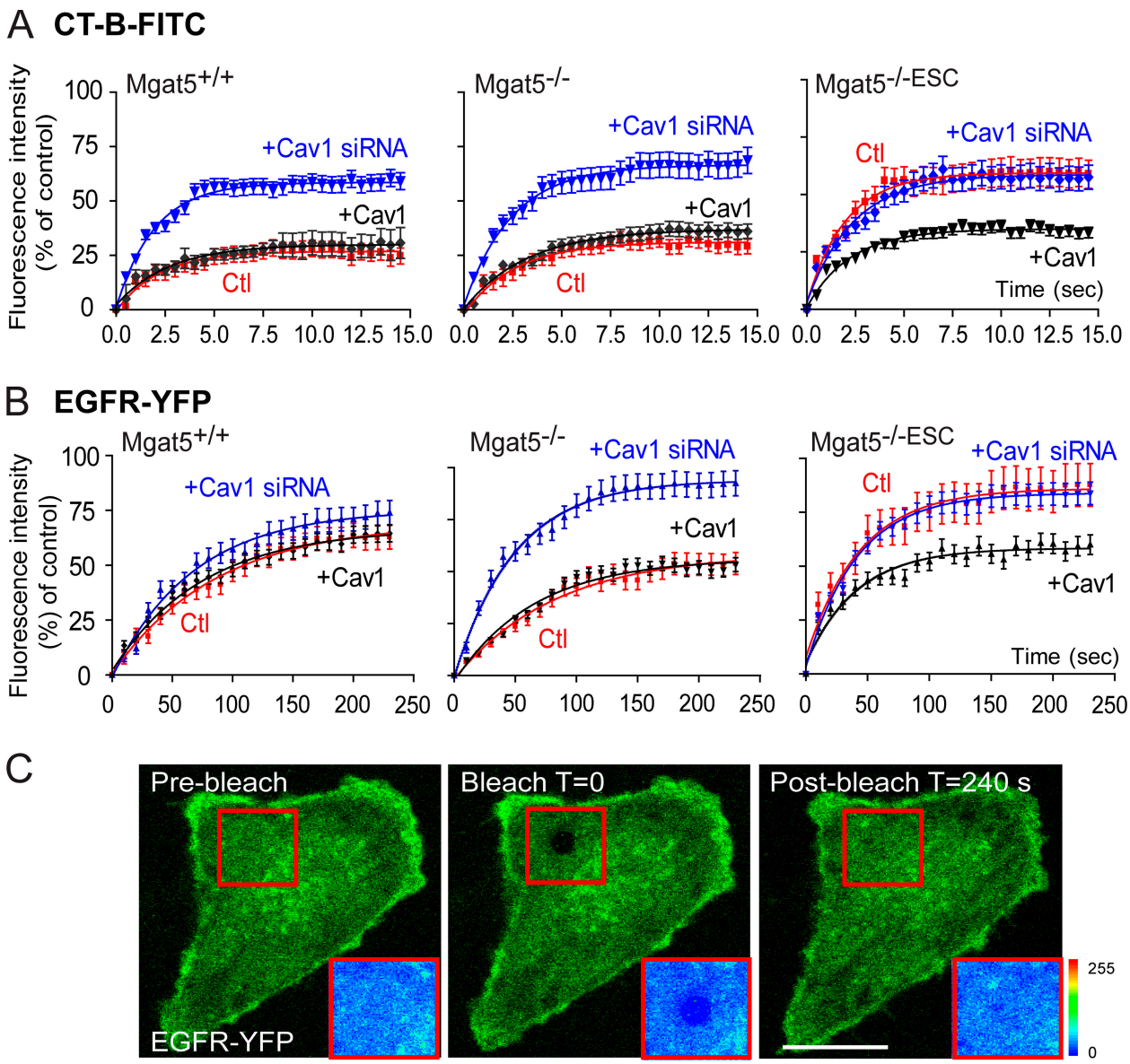

Figure 4. **Cav1 regulation of plasma membrane diffusion of CT-B–FITC and EGFR-YFP.** (A). Mgat5$^{+/+}$, Mgat5$^{-/-}$, and Mgat5$^{-/-ESC}$ cells were incubated with 5 μg/ml FITC–CT-B at room temperature, and a portion of the cytoplasm was bleached and imaged for fluorescent recovery. Percent intensity ± SEM (error bars) of FITC–CT-B in the bleached zone during recovery is shown for one representative experiment (n = 6 cells) for Mgat5$^{+/+}$ (left), Mgat5$^{-/-}$ (middle), and Mgat5$^{-/-ESC}$ (right) cells either untransfected (red) or transfected with Cav1 siRNA (blue) or Cav1-mRFP (+Cav1; black) as indicated. (B) Alternatively, Mgat5$^{+/+}$ (left), Mgat5$^{-/-}$ (middle), and Mgat5$^{-/-ESC}$ (right) cells transfected with EGFR-YFP (red) and subsequently transfected with Cav1 siRNA (blue) or infected with Cav1 adenovirus (+Cav1; black) were maintained at room temperature, and a portion of the cytoplasm was bleached and imaged for fluorescent recovery. Percent intensity ± SEM of FITC–CT-B in the bleached zone during recovery is shown for one representative experiment (n = 6 cells). See Table I for quantitative values for all conditions tested. (C) Representative images of an EGR-YFP–transfected cell are shown prebleach, immediately after bleaching (T = 0), and after recovery (240 s). Bar, 20 μM.

cells relative to Mgat5$^{-/-}$ cells by FRAP analysis (Fig. 4 B and Table I). Cav1 transfection of Mgat5$^{-/-ESC}$ cells reduced the diffusion rate and increased the immobile fraction, whereas Cav1 siRNA transfection of Mgat5$^{-/-}$ cells had the opposing effect. In contrast, modulation of Cav1 levels in Mgat5$^{+/+}$ cells by either adenoviral Cav1 expression or Cav1 siRNA did not impact EGFR-YFP diffusion (Fig. 4 B and Table I). Therefore, by limiting the exchange of EGFR-YFP between the bleached zone and the rest of the plasma membrane, Cav1 restricts EGFR mobility, but only in the absence of the Mgat5/galectin lattice.

In both Mgat5$^{+/+}$ and Mgat5$^{-/-}$ cells, Cav1 migrates at the bottom of a 5–40% sucrose gradient (Monier et al., 1995; Sargiacomo et al., 1995), which is in contrast to monomeric RhoA that migrates in lower density fractions (Fig. 5 A). In blue native gels, Cav1 migrates at ∼500 kD in both cell lines (Fig. 5 B), corresponding to the high molecular mass oligomers of Cav1 reported previously (Monier et al., 1995; Sargiacomo et al., 1995). Therefore, in spite of the reduced expression of Cav1 and caveolae, Cav1 still forms stable oligomers in Mgat5$^{-/-}$ cells. To compare the behavior of Cav1 at different expression levels, Mgat5$^{-/-ESC}$ cells were transfected with Cav1-mRFP,

Table I. **Percent mobile fraction and $t_{1/2}$ of recovery for CT-B–FITC and EGFR-YFP as determined by FRAP**

Cell transfection and/or treatment	Mgat5$^{+/+}$	Mgat5$^{-/-}$	Rescue	Mgat5$^{-/-ESC}$	ESC-Rescue
	Mf $t_{1/2}$	Mf $t_{1/2}$	Mf $t_{1/2}$	Mf $t_{1/2}$	Mf $t_{1/2}$
	% *s*	% *s*	% *s*	% *s*	% *s*
EGFR-YFP					
Control	64.8 ± 5.2 33.9 ± 1.9	60.8 ± 5.9 42.0 ± 3.3	68.6 ± 4.1 34.6 ± 4.6	83.2 ± 3.0[a] 21.0 ± 4.1[a]	68.3 ± 4.3 35.5 ± 3.7
+Cav1 adeno	57.2 ± 4.3 34.3 ± 3.2	63.5 ± 4.7 46.5 ± 3.7	63.5 ± 5.2 32.5 ± 4.0	51.1 ± 2.8[b] 37.2 ± 4.2[b]	66.5 ± 5.1 35.7 ± 4.1
+ Cav1 wt				56.5 ± 4.9[b] 35.6 ± 4.7[b]	
+Cav1 Y14F				53.6 ± 3.6[b] 36.5 ± 5.1[b]	
+Cav1 F92A/V94A				78.7 ± 4.2 24.6 ± 3.8	
+Cav1 siRNA	71.9 ± 5.0 33.6 ± 5.6	91.0 ± 2.6[a,b] 29.7 ± 4.1[b]	64.8 ± 4.8 36.5 ± 5.1	80.1 ± 4.1[a] 23.3 ± 3.6[a]	63.6 ± 4.8 36.4 ± 5.0
+Ctl siRNA	63.3 ± 4.2 33.1 ± 2.1	59.3 ± 5.7 42.2 ± 3.2	65.1 ± 4.2 34.5 ± 4.1	85.4 ± 2.7[a] 22.4 ± 3.1[a]	65.8 ± 4.6 35.5 ± 4.1
+Lactose	82.1 ± 4.7[b] 21.2 ± 2.2[b]	57.6 ± 4.7[a] 46.2 ± 4.4[a]	78.6 ± 3.6[b] 24.4 ± 4.3[b]	79.2 ± 5.1 22.9 ± 2.7	76.7 ± 4.1[b] 24.5 ± 4.0[b]
+Sucrose	60.2 ± 7.1 36.5 ± 3.4	61.6 ± 4.4 42.6 ± 4.0	66.3 ± 4.4 32.5 ± 4.2	85.2 ± 4.6[a] 21.7 ± 4.7[a]	65.3 ± 5.1 37.2 ± 4.8
+Lactose +Cav1	67.3 ± 4.0[e] 19.7 ± 1.3[b]				
	% *min*	% *min*	% *min*	% *min*	% *min*
CT-B–FITC					
Control	26.9 ± 5.6 1.7 ± 0.1	22.6 ± 5.2 1.8 ± 0.2	23.5 ± 4.2 1.7 ± 0.1	65.8 ± 4.8[a] 1.3 ± 0.2[c]	62.2 ± 5.1[a] 1.2 ± 0.3[c]
+Cav1-RFP	24.5 ± 5.6 1.8 ± 0.3	24.3 ± 3.1 1.6 ± 0.2	24.5 ± 5.0 1.8 ± 0.2	31.8 ± 6.1[b] 1.7 ± 0.1[d]	26.9 ± 5.6[b] 1.8 ± 0.2[d]
+ Cav1 WT				36.2 ± 5.0[b] 1.7 ± 0.2[d]	
+Cav1 Y14F				34.3 ± 5.3[b] 1.8 ± 0.2[d]	
+Cav1 F92A/V94A				58.2 ± 3.7 1.3 ± 0.2	
+Cav1 siRNA	60.0 ± 5.4[b] 1.1 ± 0.2[d]	71.9 ± 5.7[b] 1.2 ± 0.2[d]	66.8 ± 5.2[b] 1.1 ± 0.2[d]	61.5 ± 3.7 1.2 ± 0.2	64.7 ± 4.1 1.3 ± 0.2
+Ctl siRNA	28.8 ± 5.2 1.8 ± 0.2	22.4 ± 5.1 1.9 ± 0.3	21.9 ± 4.3 1.7 ± 0.1	62.4 ± 4.2[a] 1.3 ± 0.1[c]	66.3 ± 3.7[a] 1.2 ± 0.2[c]
+Lactose	23.3 ± 4.2 1.8 ± 0.3	23.4± 4.2 1.9 ± 0.2	22.6 ± 4.1 1.9 ± 0.3	66.9 ± 5.1[a] 1.2 ± 0.3[c]	62.4 ± 4.3[a] 1.2 ± 0.3[c]
+Sucrose	24.0 ± 4.8 1.6 ± 0.2	23.4 ± 4.6 1.8 ± 0.3	22.4 ± 5.1 1.8 ± 0.2	62.7 ± 3.9[a] 1.2 ± 0.2[c]	64.0 ± 4.9[a] 1.2 ± 0.3[c]

Mf, mobile fraction. Data are presented as means ± SEM.
[a]$P < 0.01$ compared with Mgat5$^{+/+}$(2.6).
[b]$P < 0.01$ compared with control.
[c]$P < 0.05$ compared with Mgat5$^{+/+}$(2.6).
[d]$P < 0.05$ compared with control.
[e]$P < 0.01$ compared with Mgat5$^{+/+}$(2.6) treated with lactose.

and the diffusion of Cav1 was tested by FRAP (Fig. 5 C). The transfected cells were subsequently fixed and labeled for Cav1 to compare transfected Cav1-RFP expression levels with endogenous Cav1 levels in Mgat5$^{-/-}$ and Mgat5$^{+/+}$ cells. Even when expressed at low levels, below those of Mgat5$^{+/+}$ cells, Cav1 remained highly immobile. Interestingly, the Cav1 mobile fraction but not the $t_{1/2}$ of recovery increased significantly ($P < 0.01$) with Cav1 intensity. These results indicate that even when expressed at low levels, Cav1 still forms stable oligomers at the plasma membrane.

Mgat5$^{-/-ESC}$ cells were transfected with mutants of Cav1, either a Y14F mutation of the tyrosine phosphorylation site or an F92A/V94A mutation of the scaffolding domain (Li et al., 1996; Nystrom et al., 1999). Cav1-dependent inhibition of cell

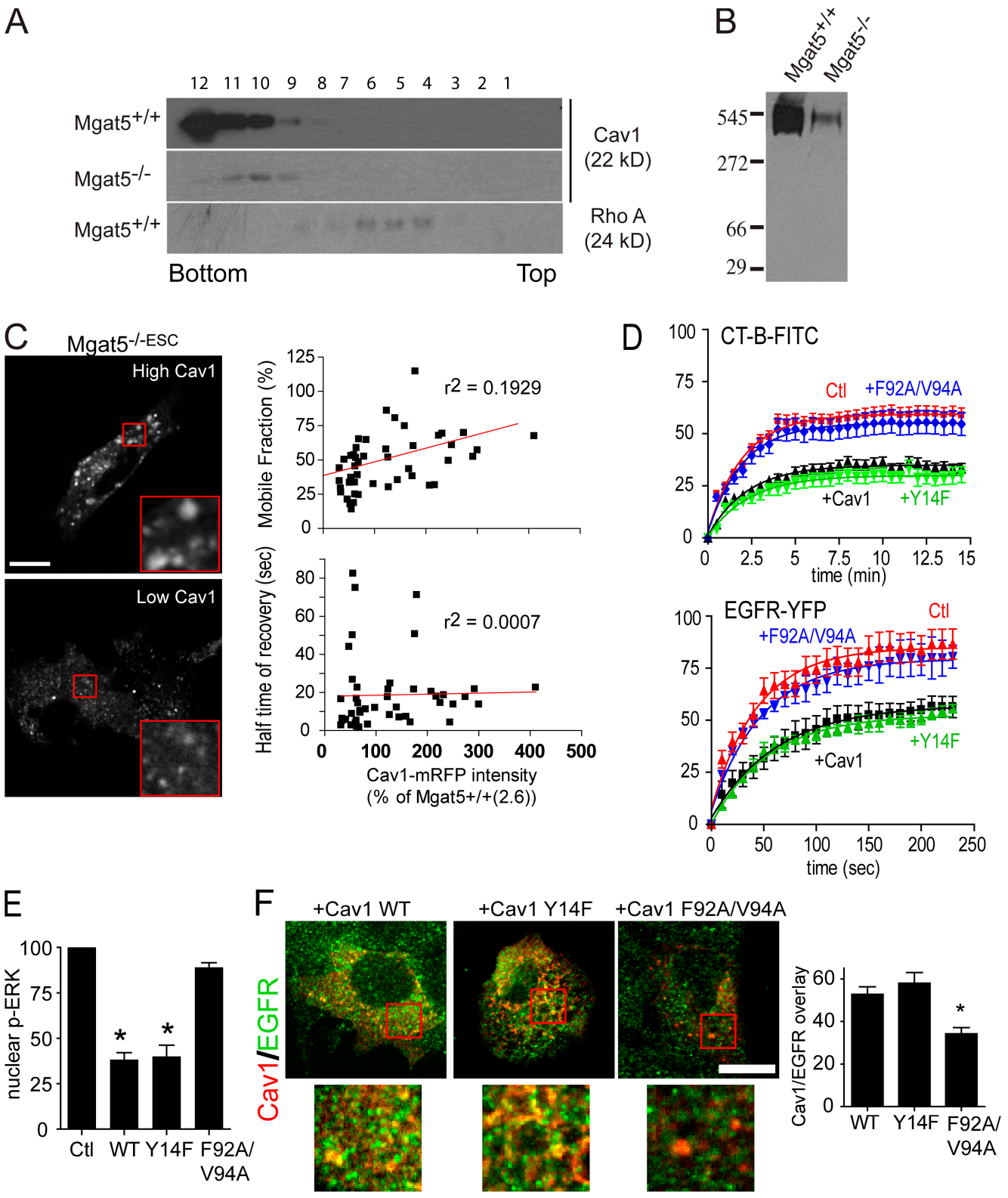

Figure 5. **Cav1 regulation of EGFR signaling and cell surface diffusion requires an intact scaffolding domain but not Y14 phosphorylation.** (A) *N*-octylglucoside lysates of Mgat5$^{+/+}$ and Mgat5$^{-/-}$ cells were analyzed by velocity sucrose gradient centrifugation, and fractions were immunoblotted for Cav1 and monomeric RhoA as indicated. Fraction 1 is the top of the gradient, and fraction 12 is the bottom. (B) *N*-octylglucoside lysates of Mgat5$^{+/+}$ and Mgat5$^{-/-}$ cells were separated on blue native gels and blotted for Cav1. (C) Mgat5$^{-/-ESC}$ cells were transfected with Cav1-mRFP, and Cav1 diffusion was assessed by FRAP. Cav1 intensity in the bleached zone was determined by comparison of Cav1 labeling intensity with RFP fluorescence in fixed cells and was normalized to Cav1 intensity in Mgat5$^{+/+}$ cells. Representative confocal images of high and low Cav1-mRFP–expressing cells are presented. Red boxed areas are enlarged in the insets to show details of Cav1 distribution. Mobile fraction (top graph) and half-time of recovery (bottom graph) in the function of Cav1 expression are presented. Linear regressions of the data points are shown as red lines. (D) Mgat5$^{-/-ESC}$ cells were co-transfected with myc-tagged Cav1 wild type, Y14F mutant, or F92A/V94A scaffolding domain mutant as well as pOCT-dsRed to identify transfected cells and were incubated with CT-B–FITC at

surface diffusion of both CT-B and EGFR-YFP (Fig. 5 D and Table I) and of EGFR signaling (Fig. 5 E) in Mgat5$^{-/-ESC}$ cells is independent of Y14F phosphorylation but requires an intact scaffolding domain. Colocalization of EGFR and Cav1 is similarly increased in Mgat5$^{-/-ESC}$ cells transfected with wild-type Cav1 and Cav1-Y14F, but the Cav1 scaffolding domain mutant shows reduced colocalization with EGFR (Fig. 5 F).

Recruitment to the galectin lattice and EGFR diffusion

The mobile EGFR-YFP fraction was significantly greater ($P < 0.01$) and the rate of recovery was significantly faster ($P < 0.01$) after photobleaching in Mgat5$^{+/+}$ cells treated with lactose than in untreated or sucrose-treated cells and was comparable with that observed in Mgat5$^{-/-ESC}$ cells (Fig. 6 A and Table I). Lactose treatment of Mgat5$^{+/+}$ also reduces Cav1 levels (Fig. 2 B). To determine whether reduced Cav1 levels are responsible for increased EGFR-YFP mobility, Cav1-transfected Mgat5$^{+/+}$ cells were treated with lactose. Cav1 overexpression increased the recruitment of EGFR to the immobile fraction but did not affect the first-order diffusion rate of EGFR compared with cells treated with lactose alone (Fig. 6 A and Table I). Disrupting the lattice with lactose did not alter CT-B diffusion in Mgat5$^{+/+}$ cells, suggesting that GM1 is not restricted by galectins (Table I). Mgat5 retroviral rescue of Mgat5$^{-/-}$ cells did not impact EGFR-YFP mobility, but the rescue of Mgat5$^{-/-ESC}$ cells, which did not restore Cav1 levels, reduced the rate of recovery and the mobile fraction of EGFR-YFP (Fig. 6 A and Table I). This confirms that galectin binding to N-glycans restricts the rate of diffusion of EGFR-YFP.

Colocalization of EGFR with Cav1 is increased in Mgat5$^{+/+}$ cells relative to Mgat5$^{-/-}$ cells, and disruption of galectin binding in Mgat5$^{+/+}$ cells with lactose but not sucrose increases EGFR colocalization with Cav1 to levels observed in Mgat5$^{-/-}$ cells (Fig. 6 B). To test Cav1 association with EGFR in live cells, Mgat5$^{-/-ESC}$ and ESC-Rescue cells were cotransfected with Cav1-CFP and EGFR-YFP, and time-lapse videos were acquired every 10 s over 5 min. Cells were fixed and labeled for Cav1 to determine relative Cav1 levels, and the mean colocalization of Cav1-CFP and EGFR-YFP was determined over the course of the video (Fig. 6 C and Videos 1–4; available at http://www.jcb.org/cgi/content/full/jcb.200611106/DC1). In ESC-Rescue cells, Cav1 association with EGFR was significantly lower ($P < 0.01$) than in Mgat5$^{-/-ESC}$ cells, irrespective of Cav1 levels. These data are consistent with the competitive exchange of EGFR between two cell surface domains: a signaling-competent Mgat5-dependent lattice and a negative regulatory Cav1-enriched microdomain.

The actin cytoskeleton restricts the mobility of EGFR-YFP in Mgat5$^{+/+}$ cells

To assess the role of the actin-based membrane skeleton on EGFR-YFP diffusion, the actin cytoskeleton was disrupted by treatment with latrunculin A (LatA). Phalloidin labeling of LatA-treated cells shows a loss of actin stress fibers and a reduction of total F-actin in Mgat5$^{+/+}$ and Mgat5$^{-/-}$ cell lines (Fig. 7 A). Disruption of the actin cytoskeleton with LatA significantly increased ($P < 0.05$) the mobile fraction of EGFR-YFP in Mgat5$^{+/+}$ cells (Fig. 7 B and Table II). The effect of LatA on EGFR stabilization in Mgat5$^{+/+}$ was also observed in Mgat5$^{+/+}$ cells overexpressing Cav1 or transfected with Cav1 siRNA (Fig. 7 B and Table II). LatA treatment had no effect on either the rate of diffusion or the immobile fraction of EGFR in Mgat5$^{+/+}$ cells treated with lactose, or in either Mgat5$^{-/-}$ cell line (Fig. 7 C). Therefore, lattice-associated EGFR shows preferential interaction with the actin cytoskeleton relative to EGFR in the absence of the lattice. However, disruption of the actin cytoskeleton with LatA does not alter the first-order rate of EGFR diffusion. This suggests that the galectin lattice and F-actin act together to regulate the mobility of the non-Cav1–associated fraction of EGFR.

Discussion

Competition between the galectin lattice and Cav1 domains regulates EGFR signaling

In this study, we show that negative regulation of EGFR through recruitment to Cav1 microdomains is opposed by the expression of β1,6GlcNAc-branched N-glycans. Therefore, Mgat5 and Cav1 interact to regulate growth signaling and tumor progression. The galectin lattice impedes the diffusion rate of EGFR, confirming our earlier report that the lattice represents a surface microdomain that limits EGFR down-regulation by endocytosis (Partridge et al., 2004). Lactose-mediated disruption of the galectin lattice in wild-type Mgat5$^{+/+}$ cells increases EGFR first-order diffusion, whereas restoration of the lattice by Mgat5 expression in Mgat5$^{-/-ESC}$ cells restricts EGFR diffusion independently of Cav1 expression. Cav1 overexpression reduces EGFR in the mobile fraction but does not suppress the effect of lactose on the first-order rate of diffusion of EGFR dynamics. The Cav1 microdomain and galectin lattice are therefore distinct cell surface domains that differentially regulate the distribution and dynamics of EGFR.

Deletion of the EGFR cytoplasmic domain did not impact EGFR lateral mobility, leading to the suggestion that extracellular interactions constrain the lateral diffusion of EGFR

room temperature. Alternatively, myc-tagged Cav1 and mutants were cotransfected with EGFR-YFP. Percent intensity ± SEM (error bars) in the bleached zone for CT-B–FITC and EGFR-YFP during recovery is shown for one representative experiment ($n = 6$ cells). See Table I for quantitative values for all conditions tested. (E) Mgat5$^{-/-ESC}$ cells were transfected with myc-tagged Cav1 wild type (WT), Y14F mutant, or F92A/V94A scaffolding domain mutant. Cells stimulated with 100 ng/ml EGF for 5 min were fixed and stained with anti–phospho-Erk and anti-myc to identify myc-tagged Cav1-labeled cells. Nuclei were identified by Hoechst staining. Quantification of phospho-Erk nuclear translocation from confocal images is shown as a bar graph ($n = 3$; >24 cells per condition). *, $P < 0.05$. (F) Mgat5$^{-/-ESC}$ cells transfected with myc-tagged Cav1 wild type, Y14F mutant, or F92A/V94A scaffolding domain mutant were immunofluorescently labeled with anti-EGFR (green) and anti-myc to localize myc-Cav1 (red) in the absence of ligand. Red boxed areas are enlarged in the insets to reveal the incidence of colocalization. The percentage of EGFR spots that overlap with Cav1 is presented in graphic form. *, $P < 0.05$. Bars, 20 μm.

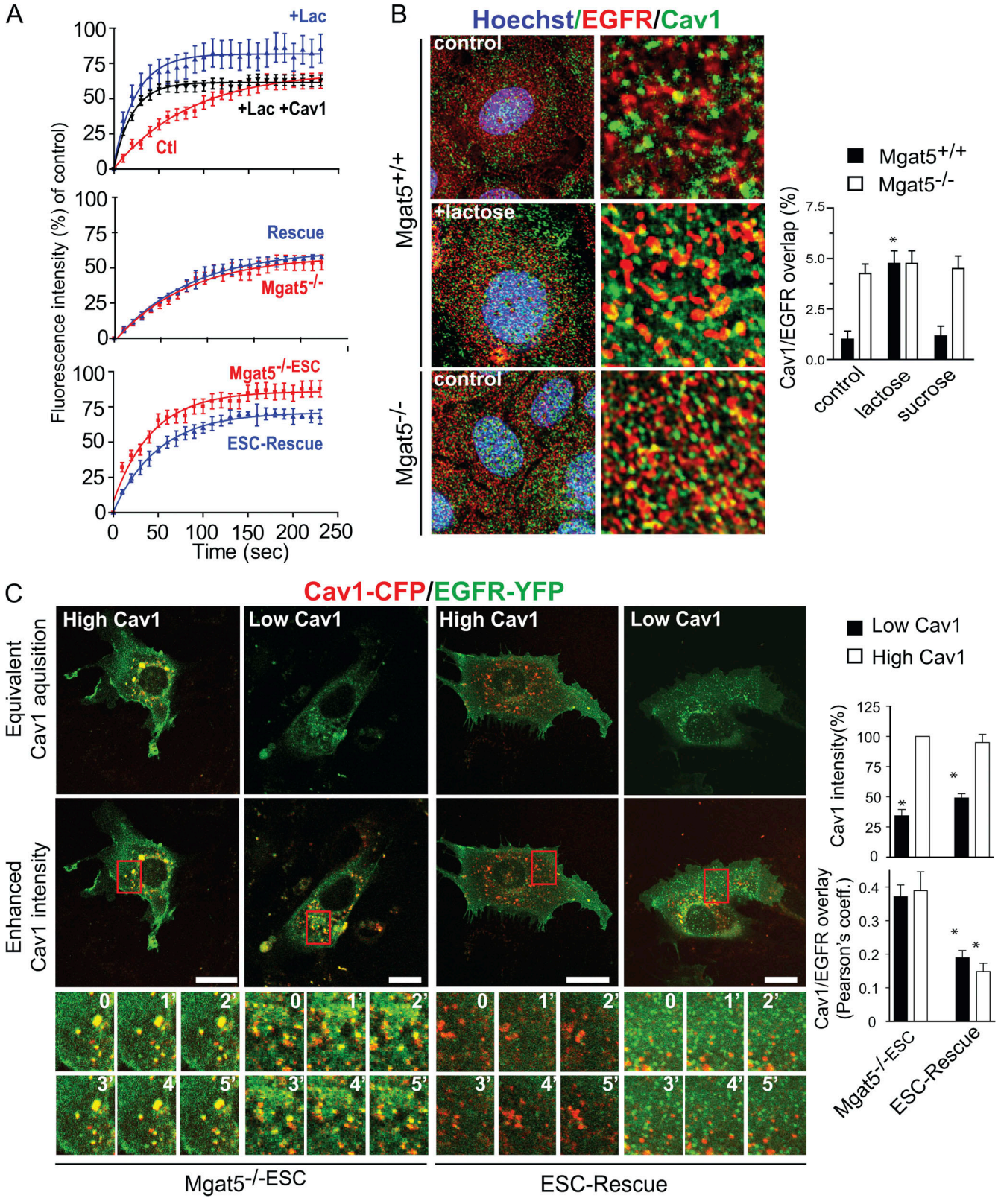

Figure 6. **The Mgat5/galectin lattice restricts EGFR diffusion and limits interaction with Cav1 domains.** (A) Percent intensity ± SEM (error bars) in the bleached zone of EGFR-YFP during recovery is shown for one representative experiment (n = 6 cells) for $Mgat5^{+/+}$ cells (top) either untreated (Ctl) or treated with 20 mM lactose (+Lac) for 48 h or infected with Cav1 adenovirus and treated with 20 mM lactose for 48 h (+Lac+Cav1). Percent intensity ± SEM in the bleached zone of EGFR-YFP during recovery is shown for one representative experiment (n = 6 cells) for $Mgat5^{-/-}$ and Rescue cells (top) and for $Mgat5^{-/-ESC}$ and ESC-Rescue cells (bottom). See Table I for quantitative values for all conditions tested. (B) $Mgat5^{+/+}$ and $Mgat5^{-/-}$ cells either untreated or pretreated for 48 h with 20 mM lactose or sucrose (not depicted) were immunofluorescently labeled for EGFR (red) and Cav1 (green) in the absence of ligand. Higher magnification images are presented to reveal the incidence of colocalization. The percentage of EGFR spots that overlap with Cav1 is

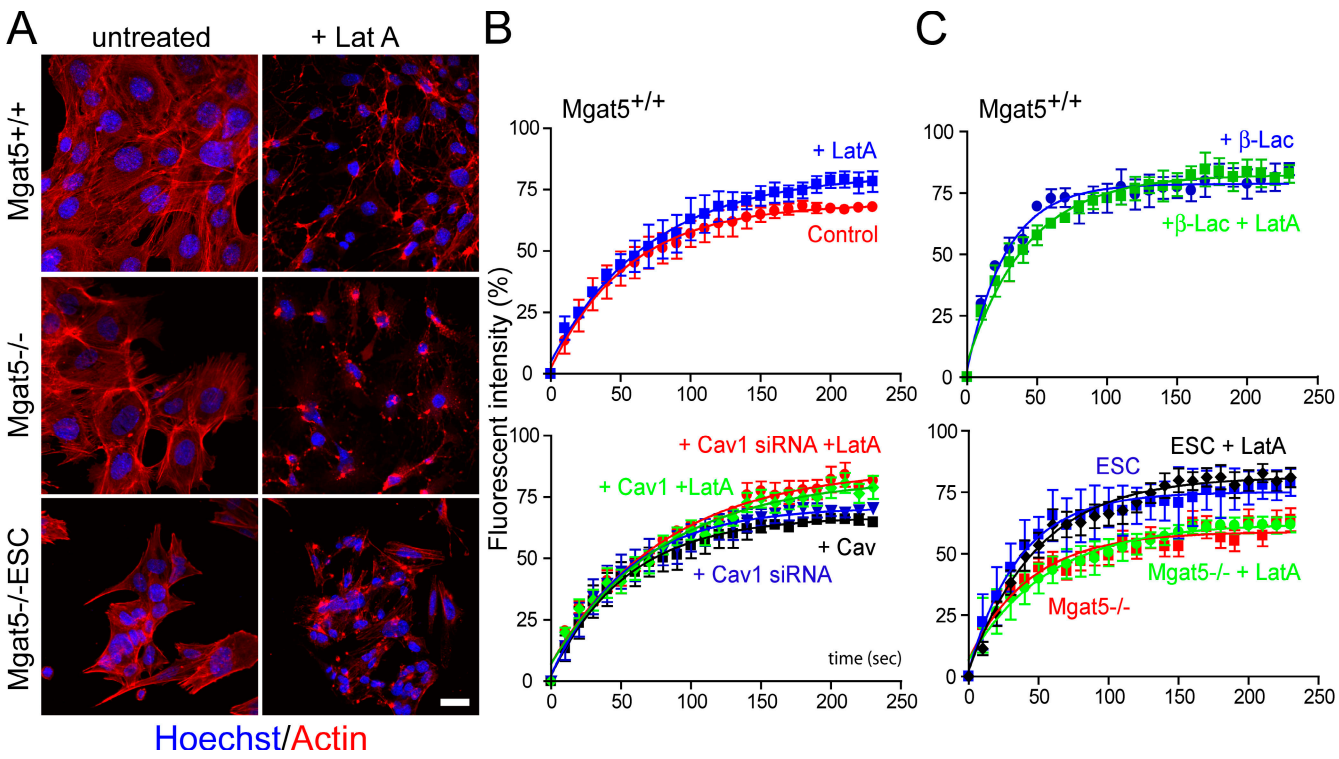

Figure 7. **The actin cytoskeleton restricts EGFR mobility.** (A) Mgat5$^{+/+}$, Mgat5$^{-/-}$, and Mgat5$^{-/-ESC}$ cells either untreated or treated with LatA for 20 min were fixed and stained with phalloidin-AlexaFluor568 (red) and Hoechst (blue). (B) Percent intensity ± SEM (error bars) in the bleached zone of transfected EGFR-YFP during recovery is shown for one representative experiment (n = 6 cells) of untreated and LatA-treated Mgat5$^{+/+}$ cells (top) or for untreated and LatA-treated Mgat5$^{+/+}$ cells infected with Cav1 adenovirus (+Cav1) or transfected with Cav1 siRNA (+Cav1 siRNA; bottom). (C) Percent intensity ± SEM in the bleached zone of transfected EGFR-YFP during recovery is shown for one representative experiment (n = 6 cells) of Mgat5$^{+/+}$ cells pretreated for 48 h with 20 mM lactose with (+Lac+LatA) or without (+Lac) Lat A (top) as well as untreated and LatA-treated (+LatA) Mgat5$^{-/-}$ and Mgat5$^{-/-ESC}$ (ESC) cells (bottom). See Table II for quantitative values for all conditions tested. Bar, 20 µm.

(Livneh et al., 1986). Mgat5 deficiency and lactose competition have previously been shown to inhibit galectin binding to EGFR (Partridge et al., 2004), identifying a requirement for extracellular galectin binding to N-glycans in the regulation of EGFR diffusion at the cell surface. We envisage that recruitment to the galectin lattice reduces the propensity of EGFR to perform hop diffusion. Disruption of the actin cytoskeleton with LatA increased the mobile fraction but not the rate of diffusion of EGFR-YFP, distinguishing its action from lactose-mediated disruption of the lattice. Although we cannot exclude the possibility of incomplete disruption of the submembrane actin cytoskeleton by LatA (Lagana et al., 2006), our data are consistent with a role for membrane protein density as a key regulator of diffusion rates in biological membranes (Fujiwara et al., 2002; Frick et al., 2007). Importantly, the effect of actin cytoskeleton disruption was not observed in Mgat5$^{-/-}$ or Mgat5$^{+/+}$ cells treated with lactose where the galectin lattice is reduced. Therefore, galectin-bound EGFR is also stabilized by the actin cytoskeleton. It is likely that galectin cross-links EGFR to other actin-associated membrane glycoproteins, generating actin-stabilized signaling domains (Fig. 8).

It is important to note that the scale of measurement with respect to both time and domain size using FRAP is dramatically larger than that measured by single-particle tracking (Kusumi et al., 2005a). Thus, it is not clear whether the Cav1-dependent immobilization of EGFR that we have measured by FRAP is equivalent to the cholesterol-dependent transient anchorage observed by single-particle tracking (Pralle et al., 2000; Dietrich et al., 2002; Ewers et al., 2005; Chen et al., 2006; Smith et al., 2006). The immobile fraction detected by FRAP in our study reflects those EGFR-YFP molecules whose interaction with other plasma membrane components, such as Cav1, the galectin lattice, or the actin cytoskeleton, constrains their ability to exchange freely with fluorescent EGFR-YFP outside the bleached region. This may not necessarily reflect stable or even direct molecular interactions but rather the preferential recruitment of EGFR to microdomains that restrict protein exchange across membrane barriers (Fig. 8).

presented in graphic form. *, P < 0.01 relative to untreated cells. (C) Time-lapse images of Mgat5$^{-/-ESC}$ and ESC-Rescue cells cotransfected with Cav1-CFP and EGFR-YFP were acquired every 10 s for 5 min. Merged images of representative cells expressing high and low Cav1-CFP levels are displayed with equivalent Cav1 acquisition settings and enhanced Cav1 intensity. Images are shown for t = 0, and higher magnifications of regions boxed in red are shown every minute for 5 min to reveal the incidence of colocalization. Cav1-CFP intensity was quantified relative to Mgat5$^{+/+}$ cells (top graph), and mean Pearson's colocalization coefficients determined from the time-lapse videos are presented for high and low Cav1-expressing cells (bottom graph). See Videos 1–4 (available at http://www.jcb.org/cgi/content/full/jcb.200611106/DC1). Error bars represent SEM. *, P < 0.01. Bars, 20 µm.

Table II. **Percent mobile fraction and $t_{1/2}$ of recovery for EGFR-YFP after treatment with LatA as determined by FRAP**

	EGFR-YFP			
	−LatA		+LatA	
	Mf	$t_{1/2}$	Mf	$t_{1/2}$
	%	min	%	min
Mgat5$^{+/+}$				
Control	65.3 ± 4.2	36.4 ± 3.7	77.4 ± 4.6[a]	37.7 ± 4.2
+Cav1 adeno	63.6 ± 5.1	34.4 ± 4.4	76.4 ± 3.2[a]	41.5 ± 5.2
+Cav1siRNA	66.2 ± 4.1	35.3 ± 4.2	74.5 ± 3.4[a]	36.7 ± 4.6
+Ctl siRNA	64.1 ± 4.2	34.5 ± 4.3	78.6 ± 3.8[a]	39.6 ± 4.4
+Lactose	80.3 ± 4.5	24.5 ± 3.1	77.4 ± 4.8	23.2 ± 3.5
+Sucrose	63.1 ± 4.6	35.9 ± 3.4	75.0 ± 4.1[a]	36.6 ± 3.0
Mgat5$^{-/-}$				
Control	62.4 ± 4.3	40.4 ± 4.5	64.5 ± 3.8	38.7 ± 3.8
Mgat5$^{-/-ESC}$				
Control	78.4 ± 5.3	22.6 ± 3.7	76.6 ± 4.9	24.5 ± 4.2

Mf, mobile fraction. Data are presented as means ± SEM.
[a]$P < 0.05$ compared with absence to LatA.

Cav1 microdomains

Activation of EGFR has been shown to occur in noncaveolar raft domains that associate with nascent coated pits (Puri et al., 2005). Similarly, in Mgat5$^{+/+}$ cells, blocking coated pit endocytosis by K^+ depletion leads to the precocious activation of Erk and growth signaling that can be suppressed by the disruption of rafts with nystatin (Partridge et al., 2004). Negative regulation of EGFR diffusion and signaling by Cav1 oligomers is consistent with the previously reported stable interaction of EGFR with Cav1 and caveolae (Couet et al., 1997; Mineo et al., 1999; Matveev and Smart, 2002). However, the ability of Cav1 to form immobile oligomers that associate with and regulate EGFR diffusion and signaling at levels below the threshold for caveolae formation argues that oligomerized Cav1 can functionally sequester EGFR independently of caveolae formation. Indeed, in endothelial cells, the overexpression of Cav1 inhibits endothelial nitric oxide synthase activity without increasing caveolae expression, suggesting that a pool of Cav1 outside of caveolae may be responsible (Bauer et al., 2005; Parton and Simons, 2007).

Freeze-etch experiments have identified a striated caveolin coat on flat membrane domains as well as caveolae (Rothberg et al., 1992), and threshold levels of Cav1 in cell surface domains are required for caveolae formation (Breuza et al., 2002). Furthermore, in contrast to the caveolae-rich basolateral surface of MDCK cells, the apical surface expresses Cav1 but no caveolae (Verkade et al., 2000). Caveolin forms stable oligomers (Monier et al., 1995; Sargiacomo et al., 1995), and the caveolin coat of vesicular transporters is highly stable (Pelkmans et al., 2004). Cav1 regulation of EGFR signaling and dynamics in Mgat5$^{-/-}$ cells that express few caveolae suggests that the regulatory function of Cav1 is dependent on Cav1 oligomerization but not necessarily on caveolae formation.

Cav1 oligomers show a reduced mobility relative to larger (more intense) Cav1 structures (Fig. 5 C), perhaps reflecting increased dynamics and exchange of Cav1 in caveolae. However, in the absence of Mgat5 expression, Cav1 at varying expression levels functions equivalently to regulate the diffusion of CT-B and EGFR as well as EGFR signaling. In blue native gel analysis, Cav1 in Mgat5$^{-/-}$ cells migrates as a sharp band, which is indicative of a highly stable oligomeric configuration. Similar SDS stable oligomers were predicted to contain 15 caveolin molecules (Monier et al., 1995). This is considerably less than the predicted 145 Cav1 molecules per caveolae (Parton et al., 2006) and is consistent with the reduced intensity and size of the Cav1 spots detected in cells expressing reduced levels of Cav1, such as Mgat5$^{-/-}$ cells. The stable interaction of EGFR with Cav1 oligomers argues that these domains form a stable platform for the recruitment of receptors and other interacting proteins. Although the spatial relationship of Cav1 oligomers, the galectin lattice, and the membrane skeleton remains uncertain, we suggest that the reduced mobility of both Cav1 oligomers and the galectin lattice is caused by the reduced ability of proteins and lipids recruited to these macromolecular domains to undergo hop diffusion (Fig. 8).

Cav1 is a conditional tumor suppressor

Spontaneous down-regulation of Cav1 in Mgat5$^{-/-}$ tumor cells argues that these conditions select for relief from the Cav1-mediated negative regulation of signaling at the cell surface. In Mgat5$^{+/+}$ cells, inhibition of the lattice with swainsonine or lactose treatment reduced Cav1 expression, whereas the Mgat5 rescue of Mgat5$^{-/-}$ cells restored Cav1 levels. This suggests that β1,6GlcNAc branching is an upstream regulator of Cav1. The inability of Mgat5 rescue to restore Cav1 levels in Mgat5$^{-/-ESC}$ cells is suggestive of Cav1 loss caused by a stable genetic change. Moreover, the inverse correlation between Cav1 levels and tumor size in Mgat5$^{-/-}$ tumors suggests that reducing Cav1 expression is one mechanism that can relieve growth restriction imposed by Mgat5 deficiency.

PyMT Mgat5$^{-/-}$ mice display a dramatic reduction in the incidence of tumor metastasis, even in those animals that develop escaper fast growth tumors (Granovsky et al., 2000). In this regard, although responsiveness to EGF is largely restored

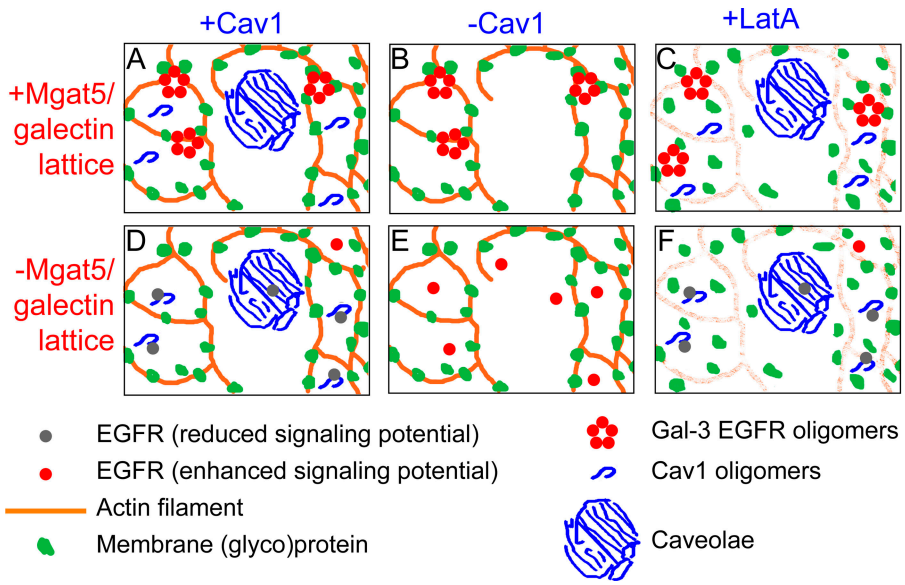

Figure 8. **Domain competition between the galectin lattice and oligomerized Cav1 microdomains regulates EGFR signaling.** In Mgat5-expressing cells, EGFR is recruited to galectin lattice domains that limit EGFR diffusion, promote interaction with the actin-based membrane skeleton, and limit interaction with negative regulatory oligomerized Cav1 microdomains (A) such that the reduction of Cav1 expression impacts neither EGFR diffusion nor signaling (B). In the absence of the Mgat5/galectin lattice, EGFR freely diffuses across membrane skeleton boundaries and is recruited to Cav1 oligomers as well as caveolae that negatively regulate signaling (D), and Cav1 down-regulation restores EGFR signaling (E). EGFR in the galectin lattice stably interacts with the membrane skeleton (A and B), and depolymerization of the actin cytoskeleton increases EGFR exchange within the galectin lattice but does not enhance the rate of EGFR diffusion or interaction with Cav1 microdomains (C and F). The diagram was adapted from Morone et al. (2006).

by Cav1 suppression in Mgat5$^{-/-ESC}$ cells, it does not rescue the lattice-dependent deficiency in TGF-β signaling, EMT, or fibronectin fibrillogenesis. This suggests that Mgat5 and β1,6GlcNAc-branched N-glycans play additional roles that are distinct from Cav1 regulation in tumor cell polarity, motility, and invasion (Cheung and Dennis, 2007).

In contrast to Mgat5$^{-/-}$ tumor cells, EGFR diffusion and responsiveness to EGF are not altered by either the overexpression or partial knockdown of Cav1 expression in Mgat5$^{+/+}$ cells. This suggests that β1,6GlcNAc-branched N- glycans and lattice retention of EGFR override negative regulation by Cav1. Although Mgat5-deficient tumor cells are partially depleted of surface EGFR as a result of constitutive endocytosis (Partridge et al., 2004), reducing Cav1 levels in the cells appears to compensate by increasing the availability of EGFR to ligand-dependent activation. We conclude that unlike Mgat5$^{-/-}$ cells, in which Cav1 expression is significantly higher ($P < 0.05$), Cav1 levels in Mgat5$^{-/-ESC}$ cells are below the threshold required for suppression, leaving an estimated 10–15,000 surface EGFRs available for optimal activation of the MAPK activation (Partridge et al., 2004; Lau et al., 2007). Surface residency of EGFR in the lattice is therefore permissive for ligand activation and limits both constitutive endocytosis (Partridge et al., 2004) and sequestration by inhibitory, immobile Cav1 domains (Fig. 8). Thus, Cav1 depletion enhances the availability of surface EGFR on Mgat5$^{-/-}$ cells, thereby removing a negative regulator of growth (Fig. 8). We suggest that Cav1 loss compensates for an approximately fivefold decrease in surface EGFR numbers observed in Mgat5$^{-/-}$ cells (Partridge et al., 2004) and is thus epistatic for EGF sensitivity.

There are only 400–800 TGF-β receptors per cell with a short surface $t_{1/2}$ (~2 h) compared with >10^5 surface EGFRs with a $t_{1/2} > 6$ h. TβRII has few N-glycans ($n = 2$) compared with EGFR ($n = 8$) and is therefore relatively more dependent on the branching of its N-glycans for residency in the lattice at the cell surface (Lau et al., 2007). In contrast, EGFR has both a greater affinity for the lattice as a result of the higher N-glycan number and a greater sensitivity to regulation by Cav1 microdomains (Fig. 1). Therefore, our data argue that affinity for the galectin lattice and Cav1-enriched microdomains partners with receptor endocytosis rates to determine receptor availability to ligand.

Finally, elevated Mgat5 expression in advanced tumors may render the suppressor function of Cav1 redundant by maintaining receptor tyrosine kinases in the galectin lattice within a physical spacing that precludes association with Cav1 microdomains. These results provide support for Cav1 as a conditional tumor suppressor, whose loss is advantageous when β1,6GlcNAc-branched N-glycans are below a threshold for optimal lattice formation. Depletion of Cav1 or increased Mgat5 expression both support early stage tumor growth; importantly, expression of the latter will permit the elevated Cav1 levels associated with poor prognosis in some tumor types.

Materials and methods

Mice and cell lines

Transgenic mice deficient in Mgat5 expression were crossed onto PyMT transgenic mice on a 129sv × FVB background (Granovsky et al., 2000). Mammary tumor samples were dissected from Mgat5$^{+/-}$ and Mgat5$^{-/-}$ mice and snap frozen on dry ice for subsequent protein extraction. Cell lines were established from solid mammary carcinoma samples dissected from either Mgat5$^{+/+}$ or Mgat5$^{-/-}$ genotypes. The cell lines used herein are designated Mgat5$^{+/+}$(2.6), Mgat5$^{+/+}$(2.8), Mgat5$^{-/-}$ (also called Mgat5$^{-/-}$(22.9)), and Mgat5$^{-/-ESC}$ (also called Mgat5$^{-/-}$(22.10)). Mgat5$^{-/-}$ and Mgat5$^{-/-ESC}$ cells genetically rescued by infection with a pMX-PIE retroviral vector for the expression of murine Mgat5 (designated Rescue and ESC-Rescue, respectively) were selected by growth in medium containing 1 μg/ml puromycin (Partridge et al., 2004). All cell lines were grown in complete medium containing DME supplemented with 10% FBS, nonessential amino acids, glutamine, vitamins, and penicillin/streptomycin in a 5% CO_2/air incubator at 37°C. For signal transduction experiments, cells were rinsed twice and incubated overnight in serum-free DME at 37°C before performing the experiment. Disruption of the actin cytoskeleton was performed by treating cells with 0.5 μM LatA in complete DME for 20 min at 37°C before experiments.

Constructs, transfection, adenoviral infection, and siRNA

EGFR-YFP was obtained from Z. Wang (University of Alberta, Edmonton, Canada), pOCT-dsRED was obtained from H. McBride (University of Ottawa, Ottawa, Canada), and myc-tagged Cav1 wild type and the F92A/V94A

scaffolding domain mutant were obtained from M.J. Quon (National Institutes of Health, Bethesda, MD). Human Cav1 was inserted into pRFP-N1 and tyrosine(Y)14 mutated to phenylalanine (F) by using the PCR-based overlapping extension technique (forward, 5′-GGGAATTCTAGCATGTCTGGGGGCAAATACGTAGACTCGGAGGGACATCTCTTCACC-3′; reverse, 5′-GGGATCCCCAGATCCTCTTCTGAGATGAG-3′). Cells were transfected using Effectene (QIAGEN) 24 h before experiments.

Adenovirus expressing myc-tagged Cav1 under control of the tetracycline-regulated promoter was used to infect cells for 48 h as previously described (Zhang et al., 2000; Le et al., 2002). Infected cells were visualized using anti-myc (Santa Cruz Biotechnology, Inc.) antibody. To knock down Cav1 expression, cells were cultured in complete medium for 2 d before transfection with specific mouse Cav1 siRNA oligonucleotides or with control siRNA (Dharmacon, Inc.). In brief, cells were rinsed twice with serum-free DME without antibiotics, transfected with siRNA for 4 h using Dharmafect 3 transfection reagent (Dharmacon, Inc.), washed twice with complete DME, and incubated in complete media for 48 h.

Western blotting

Cells were lysed in TNTE (50 mM Tris-HCl, pH 7.4, 150 mM NaCl, 1% Triton X-100, 1 mM EDTA, and protease inhibitor cocktail [Sigma-Aldrich]). Lysate protein levels were quantified using BCA Protein Assay Reagents A and B (Pierce Chemical Co.). Western blots of 30 μg of total protein were probed with polyclonal antibodies against Cav1, Cav1/2 (Transduction Laboratories), γ-tubulin (clone GTU-88; Sigma-Aldrich), or β-actin (Sigma-Aldrich) followed by the appropriate HRP-conjugated secondary antibodies and chemiluminescence. Band intensity was quantified by densitometry with Image analysis software (Scion).

Blue native gels were performed as described previously (Ren et al., 2004). In brief, cells were lysed at 4°C in lysis buffer (500 mM 6-amino caproic acid, 2 mM EDTA, and 25 mM Bistris, pH 7.0) containing 120 mM *N*-octyl-glucoside for 30 min. Lysates were clarified by centrifugation at 13,200 rpm for 10 min. Supernatant were mixed with 1/10 vol of sample buffer containing 5% R-250 Coomassie blue and 1/10 vol glycerol. Proteins were separated on linear 4–15% acrylamide gels run at 100 V at 4°C until the dye reached the middle of the gel. Blue cathode buffer (50 mM Tricine, 15 mM Bistris, and 0.02% R-250 Coomassie blue) was then replaced with clear cathode buffer (with no Coomassie blue), and gels were run at 200 V until the dye reached the bottom of the gels. Proteins were then transferred to polyvinylidene difluoride membrane and processed for immunoblotting with Cav1 polyclonal antibody (Santa Cruz Biotechnology, Inc.).

Electron microscopy

Cells were rinsed with 0.1 mM sodium cacodylate, pH 7.3, fixed for 1 h with 2% glutaraldehyde at 4°C, rinsed with cacodylate buffer, scraped from the Petri dish, pelleted, and postfixed with 2% osmium tetroxide at 4°C. The cells were dehydrated and embedded in LR-White resin. Ultrathin sections were prepared, contrasted with uranyl acetate and lead citrate, and visualized with a CM902 or a H7600 transmission electron microscope (Carl Zeiss MicroImaging, Inc. or Hitachi, respectively). Smooth caveolar invaginations and clathrin-coated vesicles within 100 nm of the plasma membrane were counted per cell profile as previously described (Le et al., 2002).

Nuclear translocation of Erk and Smad2/3

Cells were plated in 96-well plates at 5,000 cells/well or on coverslips, serum starved for 24 h, and stimulated with EGF or TGF-β1 in DME plus 0.2% FBS. After various times with cytokine, cells were fixed for 10 min with 3.7% formaldehyde at 20°C, washed with PBS plus 1% FBS, and permeabilized using 100% MeOH for 2 min. The cells were washed three times and blocked in PBS plus 10% FBS for 1 h at 37°C. Mouse anti–phospho-Erk1/2 (Thr202/Tyr204; Sigma-Aldrich) or mouse anti-Smad2/3 (Transduction Laboratories) was added at 1/1,000 in PBS plus 10% FBS and incubated overnight at 4°C. The cells were washed three times with PBS plus 1% FBS and AlexaFluor488-labeled anti–mouse Ig (Invitrogen) added at 1/1,000 with Hoechst (1/2,000) for 1 h at 20°C. After washing three times, the plates were scanned using an ArrayScan automated fluorescence microscope (Cellomics Inc.). The difference in nuclear and cytoplasmic staining intensity was determined individually for 100 cells per well, and subtraction of total nuclear intensity values from cytoplasmic intensity values was used to represent the change in activation after the addition of cytokine. The SEM ($n = 100$) was generally <4% at each assay point.

Alternatively, cells were plated on coverslips for 24 h and transfected with either myc-tagged Cav1, Cav1Y14F, or Cav1F92AV94A or with Cav1 siRNA or control siRNA for 2 d. Cells were serum starved for 24 h before stimulation with 100 ng/ml EGF for 5 min and were fixed and labeled with mouse anti–phospho-Erk1/2 and either rabbit anti-myc (Santa Cruz Biotechnology, Inc.) or rabbit anti-Cav1 (Santa Cruz Biotechnology, Inc.) followed by Hoescht staining. Confocal images of cells mounted in Celvol 205 (Celanese Ltd.) were acquired on a confocal microscope (Fluoview 1000; Olympus) with a Uplan Apochromat 1.35 NA 60× objective (Olympus) with equivalent acquisition settings. The mean intensity of nuclear phospho-Erk was quantified by creating a mask based on Hoescht staining using ImagePro Plus software (Media Cybernetics, Inc.). Data from three independent experiments (>36 cells/condition) were compiled and normalized to $Mgat5^{+/+}$ cells stimulated for 5 min with EGF.

FRAP

FRAP analysis of cells incubated with CT-B for 3 min or transfected with EGFR-YFP was performed in regular culture media without phenol red at room temperature. Images were acquired on a confocal microscope (FV1000; Olympus) with a Uplan Apochromat 1.35 NA 60× objective (Olympus) and fully opened pinhole. Photobleaching of CT-B–FITC was performed using 10 scans with the 488-nm laser at full power within a square area 20 pixels wide. EGFR-YFP photobleaching experiments were performed using 20 scans of a 405-nm scanner laser (SIM; Olympus) at full power within a circular region of interest of 27-pixel diameter. To study the effect of Cav1 on CT-B diffusion, cells were transfected with Cav1-mRFP, Cav1Y14F-mRFP, Cav1F92AV94A-mRFP, or Cav1 siRNA 2 d before experiments. Disruption of the galectin lattice was performed by treating the cells with 20 mM β-lactose or sucrose for 2 d. To study EGFR diffusion, cells were plated for 6 h and transfected with EGFR-YFP. The next day, cells were transfected with Cav1 or control siRNA or infected with Cav1 adenovirus. After 4 h, the media was changed to complete DME or complete DME containing 20 mM β-lactose or sucrose for 2 d. Recovery data (six to eight cells from each of three independent experiments) were analyzed with Prism software (GraphPad) using nonlinear regression with a bottom to bottom + span algorithm. $t_{1/2}$ of recovery and mobile fraction were calculated as previously described (Reits and Neefjes, 2001). For experiments using myc-tagged Cav1 constructs, cells were cotransfected with either EGFR-YFP or pOCT-dsRED to visualize the transfected cells. Similarly, recovery data for transfected Cav1-mRFP in $Mgat5^{-/-ESC}$ cells were obtained by FRAP analysis at room temperature. Images were acquired with equivalent acquisition settings, and, to compare Cav1-mRFP intensity with endogenous Cav1 levels, $Mgat5^{+/+}$-, $Mgat5^{-/-}$-, and Cav1-mRFP–transfected $Mgat5^{-/-ESC}$ cells were fixed and labeled in parallel with Cav1 polyclonal antibody (Santa Cruz Biotechnology, Inc.). A graph of Cav1 intensity versus Cav1-mRFP intensity was generated for fixed $Mgat5^{-/-ESC}$ cells, and a linear regression was performed to determine the intensity of Cav1-mRFP relative to endogenous Cav1 levels in $Mgat5^{+/+}$ cells in the bleach zone of live cells that underwent FRAP analysis. FRAP data are presented in function of normalized Cav1-mRFP intensity for both the mobile fraction and half-time of recovery. r^2 values were calculated from a linear regression performed with Prism software (GraphPad).

Quantitative immunofluorescence

L-PHA and Cav1 expression levels were quantified from fluorescent images of cells mounted in Celvol 205 (Celanese Ltd.) acquired with the 60× 1.35 NA Uplan Apochromat objective (Olympus) of a confocal microscope (Fluoview 1000; Olympus). Quantification of L-PHA–FITC levels (mean density of fluorescence) was performed using ImagePro Plus software (Media Cybernetics, Inc.) from confocal images acquired with equivalent acquisition settings. Values from three independent experiments were normalized to the intensity of $Mgat5^{+/+}$ cells, and significance was determined by a *t* test. To measure EGFR colocalization with Cav1, cells were plated on glass coverslips and preincubated for 48 h with 20 mM β-lactose or sucrose in complete DME, fixed, and labeled with rabbit anti-EGFR, mouse anti-Cav1 (Invitrogen), and Hoechst. Images were acquired with a 100× NA 1.4 Plan Apochromat objective (Olympus) of a microscope (DeltaVision Restoration; Olympus), and 64-layer stacks were acquired and deconvolved with softWoRx image analysis software (Applied Precision). Colocalization was quantified in Photoshop (Adobe) by defining a box of set dimensions and scoring the incidence of yellow stain within this box from six randomly selected regions within the cytoplasm of the cell. Alternatively, cells transfected with myc-tagged Cav1 constructs were labeled with anti-myc (Upstate Biotechnology) and anti-EGFR. From confocal images of cells mounted in Celvol 205 (Celanese Ltd.) acquired with the 60× 1.35 NA objective of a confocal microscope (FV1000; Olympus), the relative intensity of myc-Cav1 associated with EGFR labeling was determined using the colocalization coefficient of ImagePro Plus imaging software (Media Cybernetics, Inc.).

To quantify EGFR-Cav1 association in live cells, Mgat5$^{-/-ESC}$ and ESC-Rescue cells were cotransfected with Cav1-CFP and EGFR-YFP. Time-lapse images of cells were acquired every 10 s for 5 min in regular culture media without phenol red at room temperature with the 60× 1.35 NA Uplan Apochromat objective of the FV1000 confocal microscope. Cav1 acquisition settings were kept constant, and high and low Cav1-CFP–expressing cells were determined relative to endogenous Cav1 levels in Mgat5$^{+/+}$ cells. The Pearson's coefficient for Cav1-CFP and EGFR-YFP was calculated from two random regions of the cell for each individual time frame, and the mean Pearson's coefficient over time was determined from three independent experiments (n >15) using ImagePro Plus software.

Cav1 oligomerization gradients

Cav1 oligomerization was determined using velocity sucrose gradient centrifugation as previously described (Monier et al., 1996). In brief, cells were grown in 100-mm Petri dishes and lysed on ice in 500 µl of lysis buffer (25 mM MES, pH 6.5, 150 mM NaCl, 60 mM *N*-octylglucoside, and protease inhibitor cocktail). This lysate was overlaid on top of 4.2 ml of a 5–30% discontinous sucrose gradient prepared in the same lysis buffer. The gradients were centrifuged in an SW55 rotor (Beckman Coulter) for 6 h at 53,000 rpm. 12 equal fractions of 392 µl were collected from the top of the gradient, and an equal volume of each fraction was analyzed by SDS-PAGE and transferred onto nitrocellulose membranes for immunoblotting with anti-Cav1 (Santa Cruz Biotechnology, Inc.) or anti-RhoA (Santa Cruz Biotechnology, Inc.) antibodies.

Online supplemental material

Videos 1–4 correspond to Fig. 6 C. Mgat5$^{-/-ESC}$ and ESC-Rescue cells were transfected with Cav1-CFP (red) and EGFR-YFP (green). Videos are of Mgat5$^{-/-ESC}$ cells expressing high (Video 1) and low (Video 2) Cav1 levels and ESC-Rescue cells expressing high (Video 3) and low (Video 4) Cav1 levels. Online supplemental material is available at http://www.jcb.org/cgi/content/full/jcb.200611106/DC1.

We thank Zhixiang Wang for the EGFR-YFP construct, Michael J. Quon for the wild-type and scaffolding domain mutant Cav1 constructs, and Heidi McBride for the pOct-dsRed. Satra Nim participated in the early stages of this study.

This research was supported by a grant from the Canadian Institutes for Health Research (CIHR) to I.R. Nabi and J.W. Dennis and a CIHR studentship to E. Partridge. P. Lajoie is a research student of the Terry Fox Foundation through an award from the National Cancer Institute of Canada. J.G. Goetz holds a doctoral fellowship from the Ministère de la Recherche et des Technologies for his doctoral studies to be submitted jointly to the Université de Montréal and the Université Louis Pasteur de Strasbourg (Unités Mixtes de Recherche Centre National de la Recherche Scientifique 7034).

Submitted: 20 November 2006
Accepted: 19 September 2007

References

Ahmad, N., H.J. Gabius, S. Andre, H. Kaltner, S. Sabesan, R. Roy, B. Liu, F. Macaluso, and C.F. Brewer. 2004. Galectin-3 precipitates as a pentamer with synthetic multivalent carbohydrates and forms heterogeneous cross-linked complexes. *J. Biol. Chem.* 279:10841–10847.

Bauer, P.M., J. Yu, Y. Chen, R. Hickey, P.N. Bernatchez, R. Looft-Wilson, Y. Huang, F. Giordano, R.V. Stan, and W.C. Sessa. 2005. Endothelial-specific expression of caveolin-1 impairs microvascular permeability and angiogenesis. *Proc. Natl. Acad. Sci. USA.*. 102:204–209.

Breuza, L., S. Corby, J.P. Arsanto, M.H. Delgrossi, P. Scheiffele, and A. Le Bivic. 2002. The scaffolding domain of caveolin 2 is responsible for its Golgi localization in Caco-2 cells. *J. Cell Sci.* 115:4457–4467.

Brewer, C.F., M.C. Miceli, and L.G. Baum. 2002. Clusters, bundles, arrays and lattices: novel mechanisms for lectin-saccharide-mediated cellular interactions. *Curr. Opin. Struct. Biol.* 12:616–623.

Capozza, F., T.M. Williams, W. Schubert, S. McClain, B. Bouzahzah, F. Sotgia, and M.P. Lisanti. 2003. Absence of Caveolin-1 sensitizes mouse skin to carcinogen-induced epidermal hyperplasia and tumor formation. *Am. J. Pathol.* 162:2029–2039.

Chen, Y., W.R. Thelin, B. Yang, S.L. Milgram, and K. Jacobson. 2006. Transient anchorage of cross-linked glycosyl-phosphatidylinositol-anchored proteins depends on cholesterol, Src family kinases, caveolin, and phosphoinositides. *J. Cell Biol.* 175:169–178.

Cheung, P., and J.W. Dennis. 2007. Mgat5 and Pten interact to regulate cell growth and polarity. *Glycobiology*. 17:767–773.

Couet, J., M. Sargiacomo, and M.P. Lisanti. 1997. Interaction of a receptor tyrosine kinase, EGF-R, with caveolins. Caveolin binding negatively regulates tyrosine and serine/threonine kinase activities. *J. Biol. Chem.* 272:30429–30438.

Demetriou, M., M. Granovsky, S. Quaggin, and J.W. Dennis. 2001. Negative regulation of T-cell activation and autoimmunity by Mgat5 N-glycosylation. *Nature*. 409:733–739.

Dennis, J.W., J. Pawling, P. Cheung, E. Partridge, and M. Demetriou. 2002. UDP-N-acetylglucosamine:alpha-6-D-mannoside beta1,6 N-acetylglucosaminyltransferase V (Mgat5) deficient mice. *Biochim. Biophys. Acta*. 1573:414–422.

Di Guglielmo, G.M., C. Le Roy, A.F. Goodfellow, and J.L. Wrana. 2003. Distinct endocytic pathways regulate TGF-beta receptor signalling and turnover. *Nat. Cell Biol.* 5:410–421.

Dietrich, C., B. Yang, T. Fujiwara, A. Kusumi, and K. Jacobson. 2002. Relationship of lipid rafts to transient confinement zones detected by single particle tracking. *Biophys. J.* 82:274–284.

Edidin, M., S.C. Kuo, and M.P. Sheetz. 1991. Lateral movements of membrane glycoproteins restricted by dynamic cytoplasmic barriers. *Science*. 254:1379–1382.

Ewers, H., A.E. Smith, I.F. Sbalzarini, H. Lilie, P. Koumoutsakos, and A. Helenius. 2005. Single-particle tracking of murine polyoma virus-like particles on live cells and artificial membranes. *Proc. Natl. Acad. Sci. USA.*. 102:15110–15115.

Fra, A.M., E. Williamson, K. Simons, and R.G. Parton. 1995. *De novo* formation of caveolae in lymphocytes by expression of VIP21-caveolin. *Proc. Natl. Acad. Sci. USA.*. 92:8655–8659.

Frick, M., K. Schmidt, and B.J. Nichols. 2007. Modulation of lateral diffusion in the plasma membrane by protein density. *Curr. Biol.* 17:462–467.

Fujiwara, T., K. Ritchie, H. Murakoshi, K. Jacobson, and A. Kusumi. 2002. Phospholipids undergo hop diffusion in compartmentalized cell membrane. *J. Cell Biol.* 157:1071–1082.

Gaidarov, I., F. Santini, R.A. Warren, and J.H. Keen. 1999. Spatial control of coated-pit dynamics in living cells. *Nat. Cell Biol.* 1:1–7.

Granovsky, M., J. Fata, J. Pawling, W.J. Muller, R. Khokha, and J.W. Dennis. 2000. Suppression of tumor growth and metastasis in Mgat5-deficient mice. *Nat. Med.* 6:306–312.

Hancock, J.F. 2006. Lipid rafts: contentious only from simplistic standpoints. *Nat. Rev. Mol. Cell Biol.* 7:456–462.

Hayashi, K., S. Matsuda, K. Machida, T. Yamamoto, Y. Fukuda, Y. Nimura, T. Hayakawa, and M. Hamaguchi. 2001. Invasion activating caveolin-1 mutation in human scirrhous breast cancers. *Cancer Res.* 61:2361–2364.

Heuser, J.E., and M.W. Kirschner. 1980. Filament organization revealed in platinum replicas of freeze-dried cytoskeletons. *J. Cell Biol.* 86:212–234.

Hirabayashi, J., T. Hashidate, Y. Arata, N. Nishi, T. Nakamura, M. Hirashima, T. Urashima, T. Oka, M. Futai, W.E. Muller, et al. 2002. Oligosaccharide specificity of galectins: a search by frontal affinity chromatography. *Biochim. Biophys. Acta*. 1572:232–254.

Jacobson, K., E.D. Sheets, and R. Simson. 1995. Revisiting the fluid mosaic model of membranes. *Science*. 268:1441–1442.

Kusumi, A., I. Koyama-Honda, and K. Suzuki. 2004. Molecular dynamics and interactions for creation of stimulation-induced stabilized rafts from small unstable steady-state rafts. *Traffic*. 5:213–230.

Kusumi, A., H. Ike, C. Nakada, K. Murase, and T. Fujiwara. 2005a. Single-molecule tracking of membrane molecules: plasma membrane compartmentalization and dynamic assembly of raft-philic signaling molecules. *Semin. Immunol.* 17:3–21.

Kusumi, A., C. Nakada, K. Ritchie, K. Murase, K. Suzuki, H. Murakoshi, R.S. Kasai, J. Kondo, and T. Fujiwara. 2005b. Paradigm shift of the plasma membrane concept from the two-dimensional continuum fluid to the partitioned fluid: high-speed single-molecule tracking of membrane molecules. *Annu. Rev. Biophys. Biomol. Struct.* 34:351–378.

Lagana, A., J.G. Goetz, P. Cheung, A. Raz, J.W. Dennis, and I.R. Nabi. 2006. Galectin binding to Mgat5-modified N-glycans regulates fibronectin matrix remodeling in tumor cells. *Mol. Cell. Biol.* 26:3181–3193.

Lau, K.S., E.A. Partridge, A. Grigorian, C.I. Silvescu, V.N. Reinhold, M. Demetriou, and J.W. Dennis. 2007. Complex N-glycan number and degree of branching cooperate to regulate cell proliferation and differentiation. *Cell*. 129:123–134.

Le, P.U., G. Guay, Y. Altschuler, and I.R. Nabi. 2002. Caveolin-1 is a negative regulator of caveolae-mediated endocytosis to the endoplasmic reticulum. *J. Biol. Chem.* 277:3371–3379.

Lee, H., D.S. Park, B. Razani, R.G. Russell, R.G. Pestell, and M.P. Lisanti. 2002. Caveolin-1 mutations (P132L and Null) and the pathogenesis of breast cancer: caveolin-1 (p132l) behaves in a dominant-negative manner and caveolin-1 (−/−) null mice show mammary epithelial cell hyperplasia. *Am. J. Pathol.* 161:1357–1369.

Li, S., R. Seitz, and M.P. Lisanti. 1996. Phosphorylation of caveolin by src tyrosine kinases. The alpha-isoform of caveolin is selectively phosphorylated by v-Src in vivo. *J. Biol. Chem.* 271:3863–3868.

Livneh, E., M. Benveniste, R. Prywes, S. Felder, Z. Kam, and J. Schlessinger. 1986. Large deletions in the cytoplasmic kinase domain of the epidermal growth factor receptor do not affect its laternal mobility. *J. Cell Biol.* 103:327–331.

Matveev, S.V., and E.J. Smart. 2002. Heterologous desensitization of EGF receptors and PDGF receptors by sequestration in caveolae. *Am. J. Physiol. Cell Physiol.* 282:C935–C946.

Mayor, S., and M. Rao. 2004. Rafts: scale-dependent, active lipid organization at the cell surface. *Traffic*. 5:231–240.

Mineo, C., G.N. Gill, and R.G. Anderson. 1999. Regulated migration of epidermal growth factor receptor from caveolae. *J. Biol. Chem.* 274:30636–30643.

Monier, S., R.G. Parton, F. Vogel, J. Behlke, A. Henske, and T.V. Kurzchalia. 1995. VIP21-caveolin, a membrane protein constituent of the caveolar coat, oligomerizes in vivo and in vitro. *Mol. Biol. Cell*. 6:911–927.

Monier, S., D.J. Dietzen, W.R. Hastings, D.M. Lublin, and T.V. Kurzchalia. 1996. Oligomerization of VIP21-caveolin in vitro is stabilized by long chain fatty acylation or cholesterol. *FEBS Lett.* 388:143–149.

Morone, N., T. Fujiwara, K. Murase, R.S. Kasai, H. Ike, S. Yuasa, J. Usukura, and A. Kusumi. 2006. Three-dimensional reconstruction of the membrane skeleton at the plasma membrane interface by electron tomography. *J. Cell Biol.* 174:851–862.

Murakoshi, H., R. Iino, T. Kobayashi, T. Fujiwara, C. Ohshima, A. Yoshimura, and A. Kusumi. 2004. Single-molecule imaging analysis of Ras activation in living cells. *Proc. Natl. Acad. Sci. USA.*. 101:7317–7322.

Nichols, B.J., A.K. Kenworthy, R.S. Polishchuk, R. Lodge, T.H. Roberts, K. Hirschberg, R.D. Phair, and J. Lippincott-Schwartz. 2001. Rapid cycling of lipid raft markers between the cell surface and Golgi complex. *J. Cell Biol.* 153:529–541.

Nieminen, J., A. Kuno, J. Hirabayashi, and S. Sato. 2007. Visualization of galectin-3 oligomerization on the surface of neutrophils and endothelial cells using fluorescence resonance energy transfer. *J. Biol. Chem.* 282:1374–1383.

Nystrom, F.H., H. Chen, L.N. Cong, Y. Li, and M.J. Quon. 1999. Caveolin-1 interacts with the insulin receptor and can differentially modulate insulin signaling in transfected Cos-7 cells and rat adipose cells. *Mol. Endocrinol.* 13:2013–2024.

Okamoto, T., A. Schlegel, P.E. Scherer, and M.P. Lisanti. 1998. Caveolins, a family of scaffolding proteins for organizing preassembled signaling complexes at the plasma membrane. *J. Biol. Chem.* 273:5419–5422.

Parton, R.G., and K. Simons. 2007. The multiple faces of caveolae. *Nat. Rev. Mol. Cell Biol.* 8:185–194.

Parton, R.G., M. Hanzal-Bayer, and J.F. Hancock. 2006. Biogenesis of caveolae: a structural model for caveolin-induced domain formation. *J. Cell Sci.* 119:787–796.

Partridge, E.A., C. Le Roy, G.M. Di Guglielmo, J. Pawling, P. Cheung, M. Granovsky, I.R. Nabi, J.L. Wrana, and J.W. Dennis. 2004. Regulation of cytokine receptors by Golgi N-glycan processing and endocytosis. *Science*. 306:120–124.

Pelkmans, L., T. Burli, M. Zerial, and A. Helenius. 2004. Caveolin-stabilized membrane domains as multifunctional transport and sorting devices in endocytic membrane traffic. *Cell*. 118:767–780.

Plowman, S.J., C. Muncke, R.G. Parton, and J.F. Hancock. 2005. H-ras, K-ras, and inner plasma membrane raft proteins operate in nanoclusters with differential dependence on the actin cytoskeleton. *Proc. Natl. Acad. Sci. USA.* 102:15500–15505.

Pralle, A., P. Keller, E.-L. Florin, K. Simons, and J.K.H. Horber. 2000. Sphingolipid-cholesterol rafts diffuse as small entities in the plasma membrane of mammalian cells. *J. Cell Biol.* 148:997–1008.

Puri, C., D. Tosoni, R. Comai, A. Rabellino, D. Segat, F. Caneva, P. Luzzi, P.P. Di Fiore, and C. Tacchetti. 2005. Relationships between EGFR signaling-competent and endocytosis-competent membrane microdomains. *Mol. Biol. Cell*. 16:2704–2718.

Razani, B., Y. Altschuler, L. Zhu, R.G. Pestell, K.E. Mostov, and M.P. Lisanti. 2000. Caveolin-1 expression is down-regulated in cells transformed by the human papilloma virus in a p53-dependent manner. Replacement of caveolin-1 expression suppresses HPV-mediated cell transformation. *Biochemistry*. 39:13916–13924.

Razani, B., X.L. Zhang, M. Bitzer, G. von Gersdorff, E.P. Bottinger, and M.P. Lisanti. 2001. Caveolin-1 regulates transforming growth factor (TGF)-beta/SMAD signaling through an interaction with the TGF-beta type I receptor. *J. Biol. Chem.* 276:6727–6738.

Reits, E.A., and J.J. Neefjes. 2001. From fixed to FRAP: measuring protein mobility and activity in living cells. *Nat. Cell Biol.* 3:E145–E147.

Ren, X., A.G. Ostermeyer, L.T. Ramcharan, Y. Zeng, D.M. Lublin, and D.A. Brown. 2004. Conformational defects slow Golgi exit, block oligomerization, and reduce raft affinity of caveolin-1 mutant proteins. *Mol. Biol. Cell*. 15:4556–4567.

Rothberg, K.G., J.E. Heuser, W.C. Donzell, Y.-S. Ying, J.R. Glenney, and R.G.W. Anderson. 1992. Caveolin, a protein component of caveolae membrane coats. *Cell*. 68:673–682.

Sargiacomo, M., P.E. Scherer, Z. Tang, E. Kubler, K.S. Song, M.C. Sanders, and M.P. Lisanti. 1995. Oligomeric structure of caveolin: implications for caveolae membrane organization. *Proc. Natl. Acad. Sci. USA.* 92:9407–9411.

Savage, K., M.B.K. Lambros, D. Robertson, R.L. Jones, C. Jones, A. Mackay, M. James, J.L. Hornick, E.M. Pereira, F. Milanezi, et al. 2007. Caveolin 1 is overexpressed and amplified in a subset of basal-like and metaplastic breast carcinomas: a morphologic, ultrastructural, immunohistochemical, and in situ hybridization analysis. *Clin. Cancer Res.* 13:90–101.

Simons, K., and D. Toomre. 2000. Lipid rafts and signal transduction. *Nat. Rev. Mol. Cell Biol.* 1:31–39.

Smart, E.J., G.A. Graf, M.A. McNiven, W.C. Sessa, J.A. Engelman, P.E. Scherer, T. Okamoto, and M.P. Lisanti. 1999. Caveolins, liquid-ordered domains, and signal transduction. *Mol. Cell. Biol.* 19:7289–7304.

Smith, S.M.L., Y. Lei, J. Liu, M.E. Cahill, G.M. Hagen, B.G. Barisas, and D.A. Roess. 2006. Luteinizing hormone receptors translocate to plasma membrane microdomains after binding of human chorionic gonadotropin. *Endocrinology*. 147:1789–1795.

Suzuki, K.G., T.K. Fujiwara, M. Edidin, and A. Kusumi. 2007a. Dynamic recruitment of phospholipase C gamma at transiently immobilized GPI-anchored receptor clusters induces IP3-Ca2+ signaling: single-molecule tracking study 2. *J. Cell Biol.* 177:731–742.

Suzuki, K.G., T.K. Fujiwara, F. Sanematsu, R. Iino, M. Edidin, and A. Kusumi. 2007b. GPI-anchored receptor clusters transiently recruit Lyn and G alpha for temporary cluster immobilization and Lyn activation: single-molecule tracking study 1. *J. Cell Biol.* 177:717–730.

Suzuoki, M., M. Miyamoto, K. Kato, K. Hiraoka, T. Oshikiri, Y. Nakakubo, A. Fukunaga, T. Shichinohe, T. Shinohara, T. Itoh, et al. 2002. Impact of caveolin-1 expression on prognosis of pancreatic ductal adenocarcinoma. *Br. J. Cancer*. 87:1140–1144.

Thomsen, P., K. Roepstorff, M. Stahlhut, and B. van Deurs. 2002. Caveolae are highly immobile plasma membrane microdomains, which are not involved in constitutive endocytic trafficking. *Mol. Biol. Cell*. 13:238–250.

van Deurs, B., K. Roepstorff, A.M. Hommelgaard, and K. Sandvig. 2003. Caveolae: anchored, multifunctional platforms in the lipid ocean. *Trends Cell Biol.* 13:92–100.

Verkade, P., T. Harder, F. Lafont, and K. Simons. 2000. Induction of caveolae in the apical plasma membrane of Madin-Darby canine kidney cells. *J. Cell Biol.* 148:727–739.

Williams, T.M., and M.P. Lisanti. 2005. Caveolin-1 in oncogenic transformation, cancer, and metastasis. *Am. J. Physiol. Cell Physiol.* 288:C494–C506.

Williams, T.M., M.W.-C. Cheung, D.S. Park, B. Razani, A.W. Cohen, W.J. Muller, D. Di Vizio, N.G. Chopra, R.G. Pestell, and M.P. Lisanti. 2003. Loss of caveolin-1 gene expression accelerates the development of dysplastic mammary lesions in tumor-prone transgenic mice. *Mol. Biol. Cell*. 14:1027–1042.

Yang, G., L.D. Truong, T.M. Wheeler, and T.C. Thompson. 1999. Caveolin-1 expression in clinically confined human prostate cancer: a novel prognostic marker. *Cancer Res.* 59:5719–5723.

Zhang, W., B. Razani, Y. Altschuler, B. Bouzahzah, K.E. Mostov, R.G. Pestell, and M.P. Lisanti. 2000. Caveolin-1 inhibits epidermal growth factor-stimulated lamellipod extension and cell migration in metastatic mammary adenocarcinoma cells (MTLn3). Transformation suppressor effects of adenovirus-mediated gene delivery of caveolin-1. *J. Biol. Chem.* 275:20717–20725.